









REVIEW ARTICLE | APRIL 08 2024

# Recent advances in 3D printing for *in vitro* cancer models F

Special Collection: [Physics of 3D Printing](#)

Bin Zhang   ; Meagan Morgan  ; Xin Yi Teoh  ; Ruth Mackay  ; Sibylle Ermler  ; Roger Narayan  



*J. Appl. Phys.* 135, 140701 (2024)

<https://doi.org/10.1063/5.0200726>



Boost Your Optics and Photonics Measurements

Lock-in Amplifier

Zurich Instruments

[Find out more](#)

Boxcar Averager

# Recent advances in 3D printing for *in vitro* cancer models

Cite as: J. Appl. Phys. **135**, 140701 (2024); doi: [10.1063/5.0200726](https://doi.org/10.1063/5.0200726)

Submitted: 28 January 2024 · Accepted: 20 March 2024 ·

Published Online: 8 April 2024



Bin Zhang,<sup>1,2,a)</sup> Meagan Morgan,<sup>3</sup> Xin Yi Teoh,<sup>4</sup> Ruth Mackay,<sup>1,2</sup> Sibylle Ermler,<sup>2,5</sup> and Roger Narayan<sup>3,a)</sup>

## AFFILIATIONS

<sup>1</sup>Department of Mechanical and Aerospace Engineering, Brunel University London, London, United Kingdom

<sup>2</sup>Centre for Genome Engineering and Maintenance, Brunel University, London, United Kingdom

<sup>3</sup>Joint Department of Biomedical Engineering, University of North Carolina and North Carolina State University, Raleigh, North Carolina 27606, USA

<sup>4</sup>School of Pharmacy, University College London, London, United Kingdom

<sup>5</sup>Department of Life Sciences, Brunel University London, London, United Kingdom

**Note:** This paper is part of the special topic, Physics of 3D Printing.

**a)** Authors to whom correspondence should be addressed: [bin.zhang@brunel.ac.uk](mailto:bin.zhang@brunel.ac.uk) and [roger\\_narayan@unc.edu](mailto:roger_narayan@unc.edu)

## ABSTRACT

3D printing techniques allow for the precise placement of living cells, biological substances, and biochemical components, establishing themselves as a promising approach in bioengineering. Recently, 3D printing has been applied to develop human-relevant *in vitro* cancer models with highly controlled complexity and as a potential method for drug screening and disease modeling. Compared to 2D culture, 3D-printed *in vitro* cancer models more closely replicate the *in vivo* microenvironment. Additionally, they offer a reduction in the complexity and ethical issues associated with using *in vivo* animal models. This focused review discusses the relevance of 3D printing technologies and the applied cells and materials used in cutting-edge *in vitro* cancer models and microfluidic device systems. Future prospective solutions were discussed to establish 3D-printed *in vitro* models as reliable tools for drug screening and understanding cancer disease mechanisms.

© 2024 Author(s). All article content, except where otherwise noted, is licensed under a Creative Commons Attribution-NonCommercial-NoDerivs 4.0 International (CC BY-NC-ND) license (<https://creativecommons.org/licenses/by-nc-nd/4.0/>). <https://doi.org/10.1063/5.0200726>

## I. INTRODUCTION

Cancer is a significant burden of disease and a cause of death worldwide. Despite extensive research efforts over the past decades, the development of cancer treatments for many cancer types proved to be challenging due to the high tumor heterogeneity, making it difficult to find a universal treatment. Carcinogenesis, the process of cancer development during which normal cells are transformed into cancer cells, is characterized by genetic and epigenetic changes, which are accompanied by disruption of cell signaling and abnormal cell division. These processes are very complex, and the various steps in cancer development are still not fully understood. Traditional approaches to understanding cancer initiation and progression involve two-dimensional (2D) cell cultures and animal models.<sup>1,2</sup> 2D *in vitro* models are simple and more helpful in dissecting basic mechanistic changes or the effects of a treatment on individual endpoints.

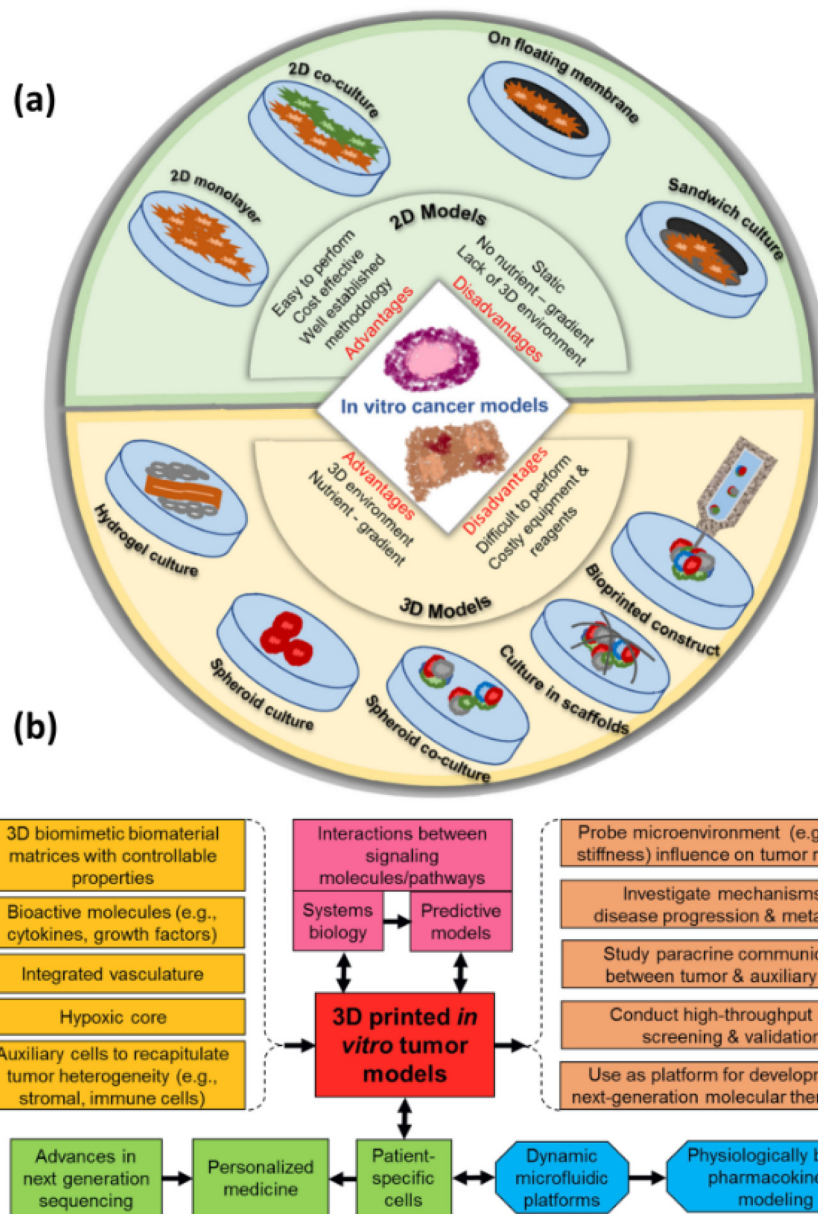
With the availability of an extensive suite of human normal tissue and cancer cell lines, as well as the increased use of primary, patient-derived cells, *in vitro* systems have the advantage of using human-relevant cells. 2D cell-culture models are suitable for high-throughput screening of various treatments under different conditions but lack the complexity of the *in vivo* context; cell-cell and cell-environment interactions in 2D are different than *in vivo*. Animal models are widely used in basic cancer research and pre-clinical testing. They are instrumental in understanding the mechanisms of tumor initiation, development, and behavior. They not only allow the study of the effect of a treatment on the tumor but also take into account pharmacokinetics and drug metabolism. However, in addition to a rise in ethical concerns about the use of animal tests, *in vivo* models are expensive and time-consuming for researchers to produce and maintain. Furthermore, animal models are not always good models for

17 April 2024 13:32:23

human physiology and often fail to recapitulate critical aspects of human tissues due to inter-species biological differences.<sup>3,4</sup>

3D printing techniques facilitate the accurate positioning of (human) cells, bioactive factors, and biomaterials, allowing for the recreation of multiple features associated with the *in vivo* tumor microenvironment.<sup>5</sup> Figure 1(a) shows the evolution of cell-culture

models from simple 2D to complex 3D-printed models. 3D-printed *in vitro* cancer or tumor models demonstrate better *in vitro* to *in vivo* correlation in drug screening, cancer metastasis, and prognosis studies. While there are several other techniques for developing 3D *in vitro* models, such as electrospinning<sup>8,9</sup> and solvent casting,<sup>10,11</sup> 3D printing offers the advantage of precisely controlling



17 April 2024 13:32:23

**FIG. 1.** (a) Various *in vitro* cancer models and evolution of cell-culture models from simple 2D to complex 3D-printed models. (b) Schematic depicting the development of 3D *in vitro* cancer models and their applications. (a) is reproduced with permission from Augustine *et al.*, *Transl. Oncol.* **14**(4), 101015 (2021); Copyright 2021 Author(s), licensed under a Creative Commons Attribution (CC BY) License.<sup>5</sup> (b) is reproduced with permission from Samavedi and Joy, *Curr. Opin. Biomed. Eng.* **2**, 35–42 (2017). Copyright 2017 Elsevier.<sup>7</sup>

the macro- and micro-inner structures of developed 3D models by depositing materials layer by layer.<sup>12–14</sup> 3D printing allows the creation of defined scaffold structures with controlled pore size and interconnectivity, as well as the ability to support cell growth and tissue formation.<sup>15–18</sup> *In vitro* tumor models created through 3D printing can function as resilient platforms for investigating disease progression mechanisms, conducting high-throughput drug screening, and facilitating the advancement of next-generation molecular therapies. Samavedi *et al.*<sup>7</sup> discussed a schematic of the development and applications of 3D tumor models, as shown in Fig. 1(b). The customization desired in the *in vitro* cancer model can be produced accurately by 3D printing. 3D printing accuracy (e.g., shape fidelity) significantly influences cancer modeling and studies using cancer models in treatment and diagnosis.

Various 3D printing applications, such as tumor organ scaffolds, 3D-printed tumor models, personalized dosage forms for drug delivery, bio-printed organs, organ-on-chip models, and devices for drug delivery and diagnosis, have demonstrated their significance in the field of medical sciences. This paper mainly focuses on the applications of 3D printing used to study *in vitro* cancer models such as the pancreas, colon, skin, liver, kidney, breast, bone, and 3D-printed microfluidic device for drug screening and delivery.

## II. 3D PRINTING TECHNIQUES FOR *IN VITRO* CANCER MODELS

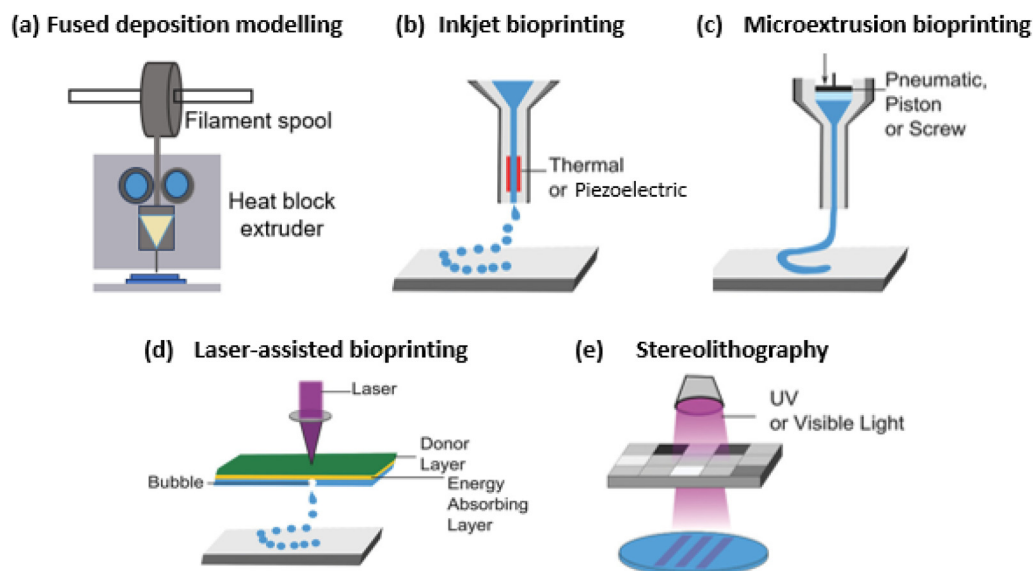
3D printing allows for modifying diverse product parameters using computer-aided design (CAD) software, including geometry, shape, size, thickness, mechanical properties, and surface properties. The CAD file is then converted into Standard Tessellation Language

(STL), a format understood by 3D printers. This technology creates reproducible complex geometries, offering the advantages of reduced manufacturing costs and time. These benefits have given rise to various 3D printing techniques, with the choice depending on the specifications and applications of the end product. Techniques like fused deposition modeling,<sup>19–21</sup> 3D bioprinting,<sup>12,22–25</sup> and stereolithography<sup>26–28</sup> have been applied to develop *in vitro* cancer models.

### A. Fused deposition modeling

Fused deposition modeling (FDM) is a 3D printing technology that involves the layer-by-layer deposition of melted thermoplastic material filaments to create three-dimensional objects.<sup>19</sup> The filament is typically heated to a molten state and subsequently extruded through the nozzle of the 3D printer, as depicted in Fig. 2(a). Continuous feeding of the filament through the extruder and nozzle is achieved by the two rollers rotating in opposite directions. The nozzle head moves with three degrees of freedom to deposit the extruded molten on the build plate per the engineered programming language (e.g., G-code) instructions.

The extrusions are sequentially deposited on the build plate, layer by layer, until the desired shape and size of the product are attained. Throughout the layering process, the printer nozzle moves back and forth based on the spatial coordinates outlined in the original CAD model within the G-code files. This continuous navigation ensures the final component matches the specified size and shape.<sup>21,30</sup> In certain FDM 3D printers, the use of multiple extrusion nozzles becomes feasible, particularly when creating components with compositional gradients.<sup>15,30,31</sup> The effectiveness and



17 April 2024 13:32:23

**FIG. 2.** Schematic of 3D printing techniques used for cancer model fabrication: (a) fused deposition modeling, (b) inkjet bioprinting, (c) microextrusion bioprinting, (d) laser-assisted bioprinting, and (e) stereolithography. (b)–(e) are reproduced with permission from Foyt *et al.*, *Adv. Healthcare Mater.* 7(8), 1700939 (2018). Copyright 2018 Author(s), licensed under a Creative Commons Attribution (CC BY) license.<sup>29</sup>

resolution of the extrusion process significantly relies on the filament's properties, such as thermoplastic characteristics, and various printing parameters like nozzle size and printing speed.<sup>32,33</sup>

### B. 3D bioprinting

Bioprinting technologies are classified by the stimuli used in print deposition. They can be divided into three groups, including inkjet bioprinting (thermal and piezoelectric effects), extrusion bioprinting (pressurized air and mechanical effects), and laser-assisted bioprinting (light energy)<sup>24</sup> as shown in Figs. 2(b)–2(d). Inkjet bioprinters dispense tiny bioink droplets (10–50  $\mu\text{m}$  diameter; 1–100 pl) with controlled volumes forming part of the final construct.<sup>24</sup> There are two commonly used inkjet printing approaches: thermal inkjet printing and piezoelectric inkjet printing.<sup>34</sup> Thermal inkjet printers apply an electronic heating element in the print head, heating the bioink locally and vaporizing it to produce pulses of pressure that expel droplets from the nozzle onto a substrate. In piezoelectric inkjet printing, the formation of droplets is initiated through a piezoelectric element linked to the printing nozzle. Applying precise voltage pulses generates a pressure wave within the nozzle, leading to the expulsion of ink in the droplet form.

Extrusion-based bioprinters are equipped with pneumatic or mechanical (screw-driven or piston) bioink dispensing systems, complemented by three-axis robotic stages that facilitate precise relative motion between the printhead and substrate along the  $x$ ,  $y$ , and  $z$  axes. This system exerts robotically controlled pressure on the bioink, resulting in the continuous extrusion of cell-encapsulated cylindrical filaments from the extrusion printhead onto a substrate. The  $x$  and  $y$  stages govern the deposition and patterning of filaments in two dimensions, forming a layer. Subsequently, under the guidance of the  $z$  stage, the substrate or printhead moves along the axis to deposit another layer, which is supported by the previously deposited layer(s).<sup>22,23</sup>

Laser-assisted bioprinting uses a laser-induced forward transfer technique to pattern metal particles; it has been applied to print cells and liquid materials with cell-level resolution for tissue engineering.<sup>35</sup> Briefly, a thin layer of laser-absorbing material is coated on the ribbon, which is transparent to the laser. The bioink, which contains heat-sensitive biological materials, is then spread on the laser-absorbing material that was coated on the ribbon. A laser pulse goes through the ribbon, causing vaporization of the laser-absorbing material film and the neighboring molecular layers of the bioink, which generates vapor bubbles. The vapor bubbles cause the bioink to jet and break into droplets, which are deposited on the substrate.<sup>35,36</sup>

### C. Stereolithography

The production of 3D objects through stereolithography relies on the controlled solidification of a liquid resin via photopolymerization in a spatially directed manner.<sup>37</sup> In this process, a pattern is projected onto the resin's surface using a computer-controlled laser beam or a digital light projector with a computer-driven building stage, as illustrated in Fig. 2(e). The resin within the pattern undergoes precise solidification to a specified depth, adhering to a support platform. After the photo-polymerization of the initial layer, the platform is moved away from the surface, and the formed

layer is once again coated with liquid resin. A pattern is then cured within this second layer, ensuring strong adherence to the first layer due to the slightly greater depth of curing compared to the platform step height.<sup>26–28</sup>

## III. 3D-PRINTED *IN VITRO* CANCER MODELS

### A. Pancreas cancer model

Table I summarizes the 3D-printed *in vitro* cancer models and the applied 3D printing techniques, materials, and cells. Pancreatic ductal adenocarcinoma (PDAC) is the most common malignant cancer of the pancreas; thus, the use of emerging technologies such as bioprinting and 3D *in vitro* models is important to improve current investigations into prognosis and treatment.<sup>38–40</sup> Hakobyan *et al.* developed a 3D *in vitro* model of acinar-to-ductal metaplasia, considered an early stage of PDAC, by printing  $10 \times 10$  arrays of methacrylated gelatin (GelMA) spheroids enclosing rat acinar cells (AR4-2JB13), transdifferentiated ductal cells, or a 1:1 combination of both cell populations. A laser-assisted bioprinting (LAB) technique, also known as laser-induced forward transfer (LIFT), was used to control spheroid cell density and improve cell viability using a nozzle-free printer and optimized photoinitiator, LAP (lithium phenyl-2,4,6 trimethylbenzoylphosphinate), concentration for gelation. Ultimately, Hakobyan *et al.* created a geometrically defined, high-throughput model that demonstrated the potential role of ductal-phenotype cells in pancreatic cancer initiation and their impact on growth kinetics.<sup>38</sup> Similar bioink materials were used in another model enclosing varying ratios of human pancreatic cancer cells and normal human dermal fibroblasts (NHDFs). Huang *et al.* printed hydrogel beads using dot extrusion printing (DEP) for bead uniformity and controlled deposition by direct gel printing. As shown in Fig. 3, there is a proportional relationship between tumor growth and stromal cell concentration, signifying a stromal–cancer cell interaction within their co-culture model. The presence of stromal cells also inhibited the induction of cell death after treatment with gemcitabine, which may play a role in the dose-dependent drug sensitivity shown when introduced to this common chemotherapy pharmaceutical.<sup>39</sup>

Desmoplasia is a common pathological feature of pancreatic cancer, where around 80% of total tumor volume is stromal tissue, highlighting its key role in tumor microenvironments (TMEs).<sup>42</sup> Langer *et al.* modeled the stromal–cancer interaction in a scaffold-free tumor microenvironment using primary patient-derived tissue combined with a 1% sodium alginate and 6% gelatin hydrogel and extruded into a  $2 \times 2 \times 1 \text{ mm}^3$  structure with a cancerous core surrounded by human umbilical vein endothelial cells (HUVECs) and pancreatic stellate cells. Their model matched *in vivo* morphology and demonstrated a similar dose-dependent drug-sensitive response to gemcitabine. Langer *et al.* concluded their model allows for patient-specific tumor research and has the flexibility for adaptation using other cancerous tissues.<sup>44</sup>

A goal among all *in vitro* models is the replication of *in vivo* environments in the most accurate and reproducible manner. While GelMA is a popular hydrogel choice because of its biocompatibility, printability, and tunable biomechanical properties, novel bioinks could offer further optimization of existing 3D models. Barros *et al.* investigated a composite scaffold material of GelMA and laponite, a

17 April 2024 13:32:23

TABLE I. Summary of 3D-printed of *in vitro* cancer models and microfluidic device systems.

| Type of cancer    | 3D printing technique      | Materials  | Cells  | Key findings  | Reference |
|-------------------|----------------------------|--|--|---|-----------|
| Pancreatic cancer | Laser-assisted bioprinting | Methacrylated gelatin (GelMA)  | Rat acinar cells (AR42J-B-13)  | Mimic early stages of PDAC, 3D acinar, and ductal co-culture improves growth kinetics and EGFR translocation  | 38        |
|                   | Inkjet bioprinting         | GelMA  | Human PDAC cells (BxPC-3)  | Biomimetic ECM and tunable stroma, 3D co-culture has better anti-cancer drug sensitivity  | 39        |
|                   | Inkjet bioprinting         | Four-arm poly(ethylene glycol) maleimide (PEG-4MAL)                      | Human PDAC cells   | Tunable ECM hydrogel compatible with rapid 3D printing and ink gelation to form complex cultures  | 40        |
|                   | Microextrusion bioprinting | Alginate-carboxymethyl cellulose (alg-CMC)                               | BxPC-3   | Bioink compatible with long-term cancer cell culture  | 41        |
|                   | Microextrusion bioprinting | GelMA  | Human PDAC cells (SW-1990)   | High laponite content reduced viability but increased growth factor and tissue-remodeling genes   | 42        |
|                   | Microextrusion bioprinting | Laponite (nanoclay)  | Human PDAC cells (MIA PaCa-2)  | Compressive moduli between 2.5 and 22.5 kPa, supported cytocompatibility, matrix adhesion, proliferation  | 43        |
|                   | Microextrusion bioprinting | Cellulose nanofibrils (CNF)  | Human PDAC cells   | Primary tissue model can replicate patient-specific tumors in response to external stimuli  | 44        |
|                   | Microextrusion bioprinting | Galactoglucomannan methacrylates (GGMMAs)                                | Human PDAC cells (HPAFII) primary patient-derived xenograft-derived pancreatic tumor cells |   |           |
|                   | Microextrusion bioprinting | Gelatin  | Human PDAC cells   |   |           |
|                   | Microextrusion bioprinting | Sodium alginate  | Human PDAC cells   |   |           |
| Colorectal cancer | Inkjet bioprinting         | Polycaprolactone (PCL) Collagen type I                                   | Human CRC cells (HCT116)   | Mimic <i>in vivo</i> TME better than 2D cultures, the 3D model demonstrated improved anti-cancer drug sensitivity   | 45        |
|                   | Inkjet bioprinting         | Alginate   | HCT116   | Tunable hydrogel bead size and stiffness, suitable for early-stage CRC tumor development better than monolayers or spheroids  | 46        |
|                   | Microextrusion bioprinting | Gelatin Sodium alginate  | Primary human CRC cells  | Patient-derived 3D-printed models retain parent tumor characteristics and respond to chemotherapeutic drug therapy in a manner similar to chemotherapy clinical outcomes                  | 18        |
|                   | Microextrusion bioprinting | R-arginine, G-glycine, and D-aspartic acid (RGD) Nanofibrillar cellulose | Colorectal liver metastasis cells (CLMCs)  | Longest (6-mo.) <i>in vitro</i> culture of patient-derived 3D-printed tumors, suitable for longitudinal chemotherapeutic screening  | 47        |
| Colorectal cancer | Microextrusion bioprinting | GelMA Laponite (nanoclay)  | Human CRC cells (SW480) Primary human CRC cells (hCCC001)                                  | GelMA-nanoclay hydrogels have suitable mechanical properties and cytocompatibility; cultured spheroids showed increased stemness, consistency, yield, and sensitivity to anti-CSC therapy | 48        |
|                   | Microextrusion bioprinting | CELLINK RGD  | Human CRC cells (Caco-2) Primary human CRC cells   | Marked difference between 3D and 2D model morphology and gene expression, 3D model has decreased drug sensitivity (5-FU, CPT-11, and oxaliplatin) compared to 2D                          | 49        |

TABLE I. (Continued.)

| Type of cancer | 3D printing technique      | Materials  | Cells  | Key findings   | Reference |
|----------------|----------------------------|--|--|--|-----------|
| Skin cancer    | Microextrusion bioprinting | GelMA  | Human melanoma cells (M4A4)  | Local cell signaling regulation using programmable release capsules; model unspecific to cancer cell line  | 50        |
|                | Microextrusion bioprinting | CELLINK bioink<br>CELLINK RGD<br>GelXA   | Lung cancer cells (A549)<br>Human melanoma metastasis (Mellm, MV3dc) | Bioinks are application specific; Matrigel® has the highest viability and poorest printability; alginate-based has the lowest viability; GelMA-based has high viability and printability                         | 51        |
|                | Microextrusion bioprinting | GelXA<br>Laminink + Matrigel®<br>GelMA   | Human melanoma cells (A375)  | Co-culture with HSFs improves tumor development and drug sensitivity; mixed culture has a time-, dose-dependent drug response to luteolin  | 52        |
|                | Microextrusion bioprinting | Polyethylene glycol diacrylate (PEGDA)<br>GelMA<br>Chitosan<br>Type I collagen | Murine melanoma (B16-F10)  | Embedded bioprinting of gelatin-chitosan microparticles modifies matrix rheology and TME; antigen-specific cytotoxic T cells can migrate, invade, and induce cell death within $\mu$ POROS matrix                | 53        |
| Liver Cancer   | Microextrusion bioprinting | Gelatin<br>Fibrinogen<br>Collagen I<br>Elastin<br>Laminin<br>Enactin<br>GelMA  | Cutaneous squamous cell carcinoma (A431)                             | 3D-printed cSCC skin equivalent model similar to <i>in vivo</i> structure and gene expression; selective, dose-dependent response to 5-FU chemotherapeutic drug  | 54        |
|                | Stereolithography          | Liver decellularized extracellular matrix (lDECIM)<br>Collagen type I<br>GelMA | Human HCC cells (HepG2)  | Variable stiffness ranges from 0.5 to 15 kPa, lDECIM-based scaffolds are suitable for cirrhotic liver tissue model, increased stiffness reduces growth and upregulates invasion potential                        | 55        |
| Liver Cancer   | Inkjet bioprinting         | Collagen type I<br>GelMA   | Human HCC cells (C3A)  | 3D co-culture liver-like morphology has decreased drug sensitivity to sorafenib compared to monoculture or 3D spheroids  | 56        |
|                | Microextrusion bioprinting | Gelatin<br>Sodium alginate   | Human HCC cells (HepG2)  | 3D-printed tumor models had a stronger liver function, enhanced expression of tumor-related genes, and decreased drug sensitivity (cisplatin, sorafenib, and regorafenib) compared to 2D models                  | 57        |
| Liver Cancer   | Microextrusion bioprinting | Gelatin<br>Sodium alginate<br>Matrigel®  | Primary CCA cells (A549)   | Invasive and metastatic 3D <i>in vitro</i> model has enhanced stemness and drug sensitivity (sorafenib, cisplatin, and 5-FU) compared to the 2D model  | 58        |
|                | Microextrusion bioprinting | Gelatin<br>Sodium alginate   | Primary HCC cells  | The patient-derived 3D-printed model retains biological and genetic features of the original tumor, capable of predictive drug screening (sorafenib, regorafenib, lenvatinib, and apatinib) in long-term culture | 59        |
| Liver Cancer   | Microextrusion bioprinting | GelMA  | Human CCA cells (RBE)  | CCA-fibroblast co-culture promotes tumor cell activity; similar results with immune cell co-culture; HUVEC cells do not play a significant role in the CCA model immune microenvironment                         | 60        |

17 April 2024 13:32:23

|                                     |  |  |           |
|-------------------------------------|--|--|-----------|
| Microextrusion bioprinting          | Thermo-sensitive hydroxypropyl chitin (HPCH) Matrigel®   | Human HCC cells (SMMC-7721)  | 61        |
| Kidney cancer                       | Gelatin<br>Sodium alginate<br>Type I collagen<br>Gelatin<br>Sodium Alginate                      | Clear cell RCC (786-O) or larynx-squamous cell carcinoma (SCC38)<br>Neuroblastoma (IMR-32)<br>Human kidney fibroblasts | 62        |
| Microextrusion bioprinting          | Sodium Alginate  | Human kidney fibroblasts   | 63        |
| Magnetic bioprinting                | NanoShuttle magnetic nanoparticles with poly-L-lysine coating<br>Culture media<br>PLA/HA coating | Patient-derived pRCC cells (Cak42, SKRC39)   | 64        |
| Breast cancer                       | PLA/HA coating   | MDA-MB-231, MSCs   | 65        |
| Microextrusion bioprinting          | Chitosan/gelatin/geniposide  | Human breast cancer cells (MCF-7)  | 66        |
| Microextrusion bioprinting          | Collagen/alginate matrix bioink  | Human breast cancer cells (MCF7, SKBR3, and MDA-MB-231)  | 67        |
| Microextrusion bioprinting          | Peptide-modified alginate hydrogels  | Human mammary fibroblasts  | 68        |
| Breast cancer bone metastasis model | PEG/PEGDA/HA   | MDA-MB-231<br>Human fetal osteoblasts (hFOB5)  | 69        |
| Stereolithography                   | GelMA/HA   | MSCs or osteoblasts<br>MDA-MB-231  | 70        |
| Bone cancer                         | Alginate/gelatin/agarose   | SaOS-2   | 71 and 72 |
| Fused deposition modeling           | Poly(l-lactide)  | OS cell lines (MG-63, SaOS-2, and HOS)   | 73        |
| Microextrusion bioprinting          | Gelatin-sodium alginate  | Human lung cancer cells A549 and 95-D  | 74        |

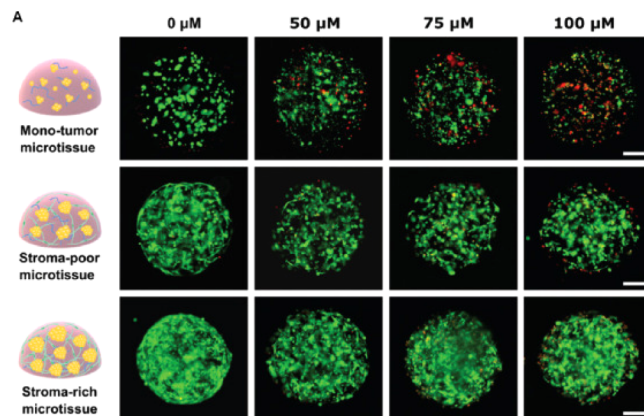


TABLE I. (Continued.)

| Type of cancer  | 3D printing technique      | Materials   | Cells   | Key findings   | Reference |
|-----------------|----------------------------|---|---|--|-----------|
|                 | Microextrusion bioprinting | Lung decellularized extracellular matrix  | Lung cancer organoids   | The lung cancer 3D model with fibrosis aids in determining suitable treatment for lung cancer patients along with fibrosis   | 17        |
|                 | Inkjet bioprinting         | Polyvinylpyrrolidone  | Human lung cell lines (A549)<br>Human lung fibroblasts (MRC5)   | 3D bio-printed triple-layered human alveolar lung models have high sustainability and repeatability  | 75        |
| Gastric cancer  | Microextrusion bioprinting | Sodium alginate<br>Gelatin (type B from bovine skin)<br>Matrigel®   | Patient-derived gastric cancer cells (GP-118)   | Performed iterative bioprinting to study spheroids for multiple generations in 3D culture conditions<br>Allow dissociation of spheroids into single-cell suspensions for reprinting into new passage models  | 76        |
|                 | Microextrusion bioprinting | Microcrystalline cellulose<br>Gastric tissue-derived decellularized extracellular matrix (g-dECM)<br>Stomach-derived decellularized extracellular matrix (st-dECM)<br>PF127 for the hollow tubular structure for blood vessel | Gastric cancer cell lines (AGS, SNU-1, and KATO3)<br>Dissociated cells from patient-derived gastric cancer tissue | Developed bioink which provides a biochemically and biophysically appropriate microenvironment for gastric cancer cell analysis which potentially be applied in the fabrication of complex gastric cancer system<br>Fabrication of the vascularized gastric cancer organoid-based model<br>Allow patient-specific chemotherapy drug screening to vascular endothelial growth factor receptor 2 (VEGFR2)-targeted therapy | 77        |
|                 | Digital light processing   | <i>cis</i> -1,4 polyisoprene (IR)<br>2-(2-ethoxyethoxy) ethyl acrylate (EOEOEA)   | <i>H. pylori</i><br>Gastric cancer cells (MKN-45)   | Development of biomimetic gastric model with fold structures, flexibility and fluid dynamics which simulates a realistic gastric track   | 78        |
| Multiple        | Stereolithography          | Photocurable plastic resin<br>Casting wax support material  | microfluidic device systems   | Fabrication of microfluidic device with high surface area and fluid flow adjustment, which increased the capture efficiency of tumor cells at around 90%<br>Isolation of circulating tumor cells (MCF-7, SW480, PC3, and 293T) from peripheral blood samples   | 79        |
|                 | Digital light processing   | Photocurable polymer urethane   | Monoclonal antibody mAb CO17-1A targeted to EpCAM<br>Colon cancer cell (Caco-2)<br>Breast cancer cell (MCF-7)     | Fabrication of immunomagnetic concentrator with high-aspect-ratio structure and high flow rates resistance, which increased the capture efficiency of tumor cells<br>Concentrated captured cells by 100 times within minutes   | 80        |
| Prostate cancer | Fused deposition modeling  | Poly(lactic acid) (PLA)   | —   | First study of cancer cell detection in blood via ATP luminescence assay<br>Increased the assay sensitivity by ten times compared to a commercial kit with conventional batch processes<br>Fabrication of the first portable microfluidic immunosensor   | 81        |

17 April 2024 13:32:23

|              |                               |  |   |    |   |
|--------------|-------------------------------|--|---|----|---|
| Lung cancer  | Inkjet printing               | NuSil medical grade silicone (MED-6033)                                  | Lung cancer cell (NCI-H1437)  | 82 | Identification of biomarker proteins associated with prostate cancer, including prostate-specific antigen (PSA), prostate-specific membrane antigen (PSMA), and platelet factor-4 (PF-4)<br>Initial utilization of supercapacitors in a voltage-driven biosensor<br>Demonstrated strong correlations with single-protein ELISA for three proteins in the serum of six patients with prostate cancer<br>Fabrication of microfluidic channel using 3D printing to produce lung-on-chip system<br>Incorporated with biosensor for real-time monitoring (pH, TEER), toxicity, drug IC50, and confocal imaging for live/dead assay |
| Liver cancer | Direct ink writing            | Human HCC (HepG2) alginate   | HepG2   | 83 | Fabrication of hepatocyte-alginate hydrogel-based construct within the chip system for drug metabolic assessment  |
|              | Inkjet printing               | Fibronectin-gelatin  | Myoblast cell (C2C12)<br>Human aortic endothelial cell<br>HepG2<br>Human umbilical vein endothelial cell (HUVEC)<br>Normal human dermal fibroblast (NHDF) | 84 | Fabrication of 3D human microtissue array by printing layer-by-layer assembly of cells and protein<br>Accommodated simplified 3D liver structure consists of hepatocytes and liver endothelial cells within the chip system<br>First report of the integration of hundreds of multilayered micro-tissues into a micro-array, which reproduced 3D cell-cell interactions similar to actual tissue/organ  |
|              | Bioprinting                   | HepG2/C3A spheroids<br>GelMA hydrogel                                    | HepG2/C3A cell  | 85 | Fabrication of long-term (30 days) functional hepatic construct culture within chip system for drug toxicity assessment<br>Dot-arrays bioprinting of spheroids-GelMA mixture using micromolds   |
|              | Bioprinting                   | PCL platform<br>Gelatin hydrogel<br>Collagen hydrogel                    | HepG2<br>HUVEC  | 86 | One-step fabrication of organ-on-chip without a secondary cell-seeding process<br>3D-bioprinted liver-on-chip showed a significant enhancement in the liver function compared to 3D-bioprinted models   |
| Brain cancer | Syringe extrusion bioprinting | Brain decellularized extracellular matrix (BdECM)<br>Collagen<br>Silicon | Glioblastoma<br>HUVEC   | 87 | Fabrication of a patient-specific glioblastoma-on-chip by incorporating robust cell heterogeneities, extracellular matrix components, and the compartmentalized tissues associated with glioblastoma<br>Proved to identify the patient-specific treatment responses, including drug combination screening   |
| Bone cancer  | Stereolithography             | GelMA<br>Hydroxyapatite (HAp)  | Lung cancer cell (A549)<br>Mesenchymal stem cell  | 88 | Fabrication of bone-mimetic microenvironmental model on-chip to study bone metastasis, dormancy, and reactivation   |



**FIG. 3.** Direct gel printed 3D PDAC hydrogel beads treated with a chemotherapy drug. Live/dead assays (calcein-AM/PI) over different stroma concentrations after one week culture and drug dosages after 72 h gemcitabine exposure. Red (propidium iodide) fluorescence indicates dead cells, and green (calcein-AM) fluorescence indicates live cells. Reproduced with permission from Huang *et al.*, *Int. J. Bioprinting* **9**(3), 1–13 (2023). Copyright 2023 Author(s), licensed under a Creative Commons Attribution (CC BY) license.<sup>39</sup>

synthetic nanosilicate known for its ability to alter ink rheology through induced shear-thinning behavior. By extruding hydrogel droplets with a 1:1 ratio of pancreatic carcinoma cells and mouse embryonic cells (to simulate fibroblasts and MSC interactions), they assessed a PDAC TME model using an optimized 10% GelMA and 1.5% laponite ink. Compared to GelMA alone, the inclusion of laponite improved mechanical and biological properties with a correlation between laponite concentration, cell aggregation, and upregulation of tumor-associated and fibroblast-associated genes linked to desmoplasia and ECM accumulation.<sup>42</sup> Habib *et al.* verified the printability of a novel 4% alginate–4% carboxymethyl cellulose (alg-CMC) hydrogel combined with human pancreatic cancer cells (BxPC3) and crosslinked via calcium chloride. A  $10 \times 10 \times 1 \text{ mm}^3$  lattice was extruded using a pneumatic extrusion bioprinter for characterization and exhibited higher cell viability after 23 days than within cell-laden alginate alone.<sup>41</sup> Utama *et al.* used PDAC cells and human dermal fibroblasts to explore another hydrogel of four-arm poly(ethylene glycol) maleimide (5% PEG-4MAL). The authors validated the ink's tunability, high cell viability, and rapid gelation, which are compatible with drop-on-demand printing methods.<sup>40</sup> Similarly, Xu *et al.* used a pancreatic tumor cell line to assess a UV cross-linkable gel comprised of cellulose nanofibrils (CNFs) and galactoglucomannan methacrylates (GGMMAs), demonstrating ink tunability to achieve a strong yet lightweight gel with adequate cell viability and ECM adhesion.<sup>43</sup>

## B. Colorectal cancer model

Colorectal cancer (CRC) is widely studied due to its high fatality and limitations in both early diagnosis and treatment. CRC is the third most common cancer type and is highly prevalent in both men and women.<sup>18,47,48</sup> Current pre-clinical models use standard

polystyrene tissue cell plates (TCPs) as cell-culture substrates; however, biofabrication has a high potential for improving the complexity and reproducibility of *in vitro* cancer models. Rosa *et al.* challenged traditional methods using inkjet microbeads to create an early-stage model of CRC using a human colorectal cancer cell line (HCT-116) in a 2% alginate solution and saw the microbeads maintained a high cell viability, increased in stemness, and reduction of hypoxia in comparison to 2D TCPs and 3D spheroids.<sup>46</sup> Chen *et al.* used a custom-built electro-hydrodynamic jet printer to extrude a collagen-PCL lattice scaffold subsequently seeded with HCT116, cancer-associated fibroblasts (CAFs), and tumor-associated endothelial cells (TECs). In comparison to 2D cultures, the 3D scaffold was more physiologically relevant and able to better mimic the *in vivo* TME indicated by increased expression of MMP-2 (matrix remodeling), CD133 (stemness), and ki67 (cancer cell proliferation), upregulation of CAF markers, and higher tumorigenicity and reduced drug sensitivity.<sup>45</sup> Sbirkov *et al.* further improved their 3D model in comparison to 2D cultures using a BioX extrusion-based bioprinter to print a simple two-layer cylindrical model of *CELLINK* RGD bioink [alginate, R-arginine, G-glycine, and D-aspartic acid (RGD)-modifier, and nanofibrillar cellulose] encapsulating Caco-2 colorectal cancer cells. A significant number of gene expression changes were seen between the two models associated with hypoxia, cell adhesion, apoptosis, and cell cycle arrest in addition to a decrease in drug sensitivity to irinotecan and 5-fluorouracil (5-FU), two standard chemotherapies.<sup>49</sup>

A major issue for CRC is metastasis and heterogeneity between patient tumors. Zhang *et al.* used a combination of the CRC line, SW480, and primary CRC cells from surgical specimens to create GelMA-laponite-based *in vitro* models to target cancer stem cells (CSCs), the source of tumor recurrence and metastasis. Figure 4 shows the 3D printing experiment setup. They found that hydrogel structures were able to induce higher CSC yield through activation of the Wnt/ $\beta$ -catenin signaling pathway and demonstrated overall improved stemness, self-renewal capabilities, and differentiation markers potentially, providing a model for CSC-targeted therapies.<sup>48</sup> Similarly, Sun *et al.* developed individualized *in vitro* models using patient-derived CRC cells in a gelatin–sodium alginate (gel-SA) ink. They compared a microextruded  $6 \times 6 \times 1.2 \text{ mm}^3$  grid model to patient-derived organoid models. While the 3D *in vitro* models depicted morphological similarities to *in vivo* tumor samples, the authors observed differences in the response of the models to chemotherapy drugs using different patient-derived cells, but a significant correlation between the personalized model and the corresponding real patient outcomes.<sup>18</sup> An important aspect of drug screening predictions is model longevity. McGuckin *et al.* aimed to create a model that could mimic patient outcomes synchronously with their treatment plan. A BioX *CELLINK* printer was used to extrude *CELLINK* RGD bioink encapsulating primary CRLM cells and tracking cell viability and therapeutic response over six months, the longest *in vitro* study to date.<sup>47</sup>

## C. Skin cancer model

Melanoma is responsible for 90% of all death-related skin tumors due to its extreme invasiveness.<sup>51</sup> 3D bioprinting techniques have been used to create proof-of-concept models targeting

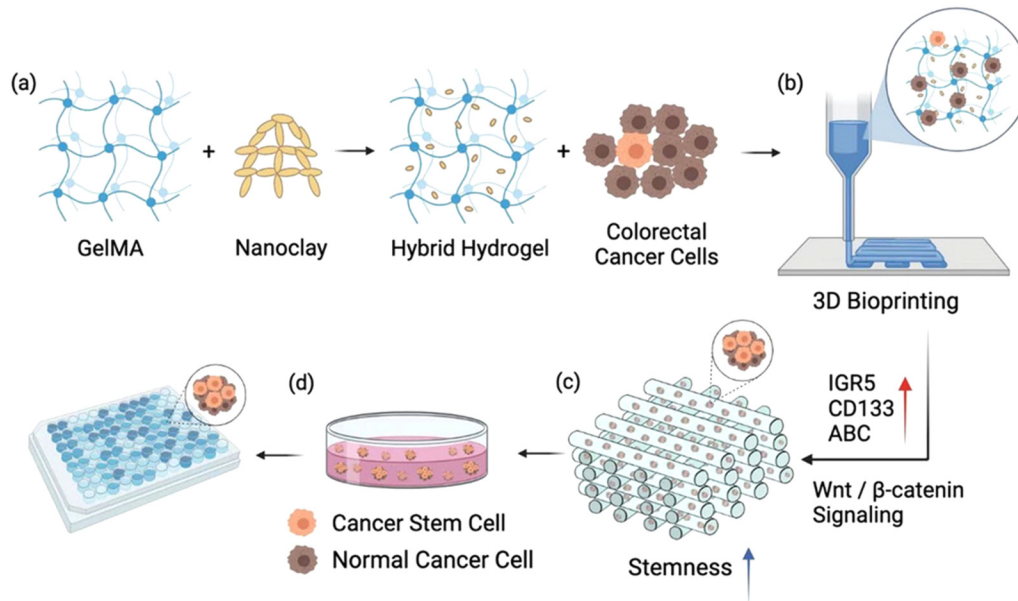


**FIG. 4.** Schematic of developing GelMA-nanoclay hydrogel lattice structures for CSC spheroid models. (a) Ink preparation, (b) extrusion bioprinting, (c) CSC enrichment, and (d) spheroid isolation for drug screening. Reproduced with permission from Zhang *et al.*, *Small* **18**(18), 2200364 (2022). Copyright 2022 John Wiley and Sons.<sup>48</sup>

a better understanding of melanoma metastasis.<sup>50,51</sup> Meng *et al.* constructed an *in vitro* vascularized tumor model of human melanoma cell (M4A4) and endothelial cell (HUVEC) droplets into GelMA matrices to explore the mechanisms of metastasis such as invasion, intravasation, and angiogenesis.<sup>50</sup> Schmidt *et al.* developed a proof-of-concept *in vitro* melanoma model to test existing limitations depending on bioink composition. Matrigel®, a gold standard for mimicking native ECM, is compared to four commercial bioinks (*CELLINK* bioink, *CELLINK* RGD, *GelXA*, and *GelXA* Laminink+). Two melanoma cell lines were assessed. Neither proliferated in the *CELLINK* bioinks in comparison to the other hydrogels, and while Matrigel® demonstrated the best cell viability, it had the poorest printability. Therefore, model results strongly depend on cell types and biomaterial composition, and these components should be specifically assigned based on model application.<sup>51</sup>

To improve model mimicry of the native TME, *in vitro* designs require increasing complexity. Sang *et al.* compared the response of a multicellular model using a human melanoma cell line and fibroblasts encapsulated within a 1:1 GelMA/PEGDA grid hydrogel to a monoculture model of the same design. The addition of fibroblasts modified the morphology, migration, proliferation, drug sensitivity, and expression levels of metastasis-related genes.<sup>52</sup> Besides cellular additions, model complexity can be increased through the selected bioprinting technique and the structure of the hydrogel matrix. Reynolds *et al.* printed a novel microporogen-structured ( $\mu$ POROS) matrix by embedding sacrificial microparticles of gelatin and chitosan within a collagen matrix as seen in Fig. 5. The embedded particles modified the rheology and porosity of the

TME, enhancing cell migration and proliferation. Additionally, they used this matrix to demonstrate antitumor targets are antigen specific. By co-culturing pmel-1 CD8+ T cells, which are known for slowing tumor growth via the pmel-17 antigen, with murine melanoma tumor cells, results showed successful cell migration, infiltration, and a volumetric reduction in tumor size compared to  $\mu$ POROS matrices with wild-type CD8+ T cells.<sup>53</sup> Browning *et al.* developed a 3D-bioprinted cutaneous squamous cell carcinoma (cSCC) skin model that included dermis, basal membrane, and epidermis layers with embedded cancerous spheroids. They used imaging biomarkers [ZsGreen green fluorescent protein (Zs-GFP) and tdTomato red fluorescent protein (tdT-RFP)] to track cell numbers within the tissue and saw a dose-dependent response to 5-FU drug treatment that decreased viable cell numbers within the cSCC models in comparison to healthy keratinocyte.<sup>54</sup>

#### D. Liver cancer model

Hepatocellular carcinoma (HCC) has the second highest mortality rate of cancers worldwide, being the fifth most common malignant cancer.<sup>55</sup> Due to the common and aggressive prognosis of HCC, many researchers work toward improving existing models used for anti-cancer drug screening.<sup>55–57,61</sup> Three-dimensional models have shown improvement over the current standard of 2D cultures and animal models, which are restricted by model morphology and species-specific biology.<sup>56–58,60,61</sup> Sun *et al.* established a 3D HCC model composed of HepG2 cells within a gel-SA hydrogel. In comparison to 2D cultured cells, the bioprinted 3D model expressed a consistently increasing growth rate over 10 days, higher

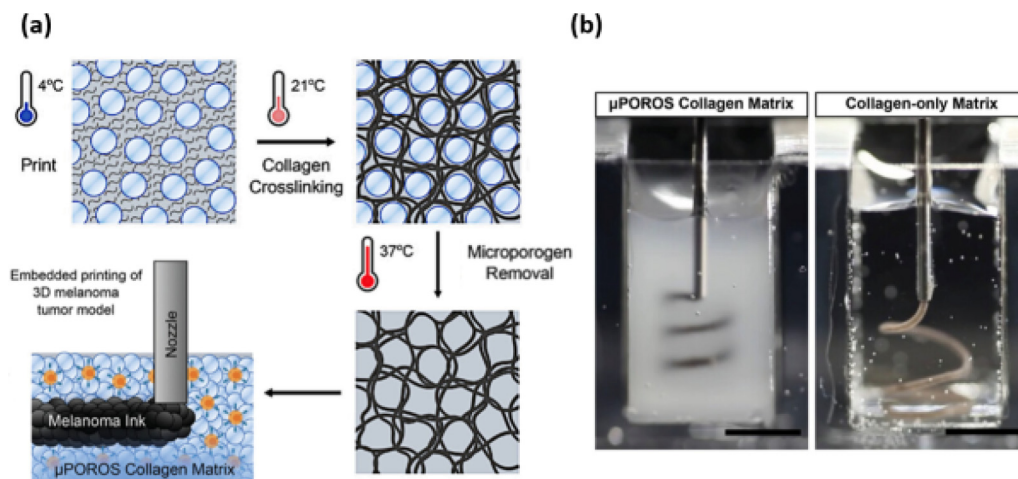


**FIG. 5.** Schematic for microporogen-structured ( $\mu$ POROS) collagen matrices for 3D-printed melanoma tumors. (a) Gelatin-chitosan sacrificial microparticles in blue with the collagen matrix in black. Melted microparticles leave gray pores behind. The melanoma bioink can be embedded within the remaining matrix structure. (b) Murine melanoma ink deposited within  $\mu$ POROS collagen vs a collagen-only matrix. Scale bar = 4 mm. Reproduced with permission from Reynolds *et al.*, *Adv. Mater.* **35**(33), 2210748 (2023). Copyright 2023 John Wiley and Sons.<sup>53</sup>

levels of tumor-related mRNA and proteins, and improved drug sensitivity to cisplatin, sorafenib, and regorafenib.<sup>57</sup> Li *et al.* compared the migration ability, protein expression, and drug response of a 3D-printed HCC co-culture model with microfluidics (3DPF) to a model without microfluidics (3DP) and a 2D planar culture. A thermo-sensitive hydroxypropyl chitin (HPCH) hydrogel combined with 10% Matrigel<sup>®</sup> was used as a bioink with encapsulated human HCC cells (C3A cell line) and peripheral blood mononuclear cells (PBMCs). An antibody drug, metuzumab, was used to assess model drug sensitivity. Unsurprisingly, the 2D model was the most sensitive and showed the least amount of migratory activity and decreased proliferation. The 3DPF model was more sensitive to drug dosage than the 3DP and a better match for previous animal models.<sup>61</sup>

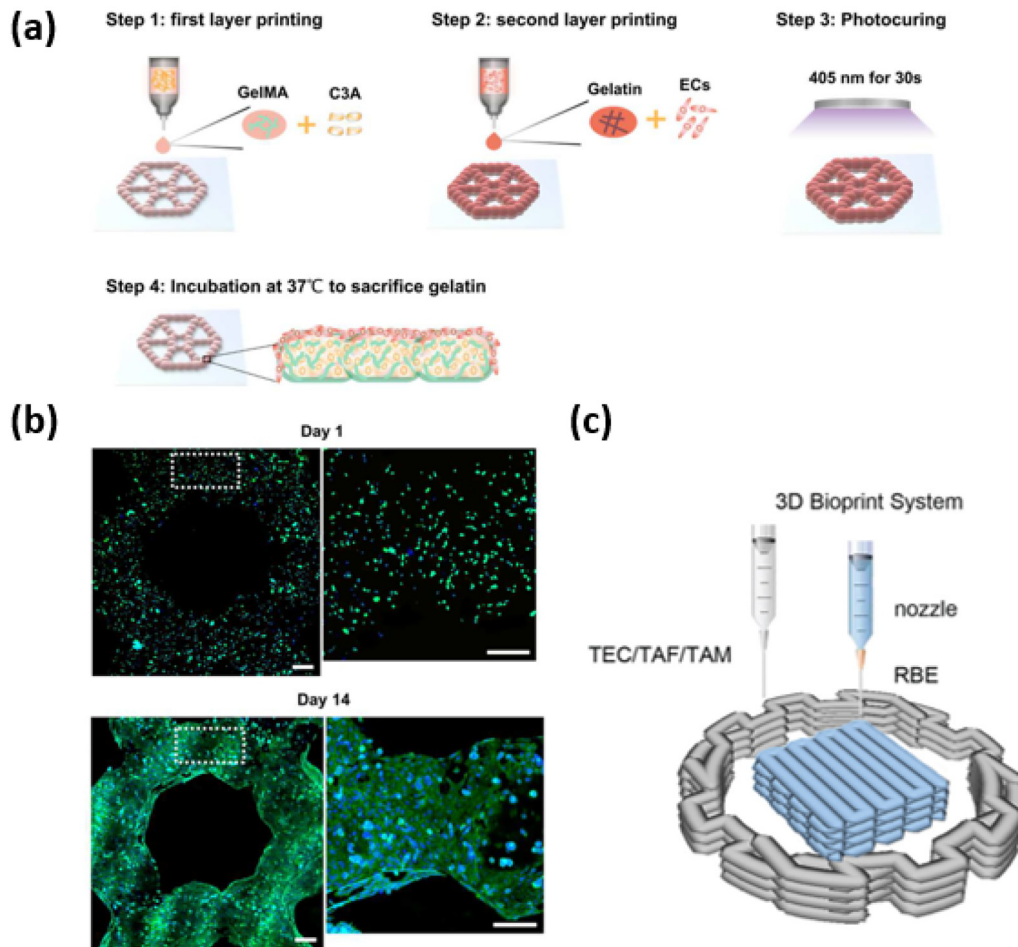
Ma *et al.* approached current *in vitro* model insufficiencies by incorporating liver-specific decellularized extracellular matrix (dECM) into a 5% GelMA bioink to emulate the distinct biochemical properties of the hepatic *in vivo* microenvironments. The HepG2 hepatocellular carcinoma line was printed into a three-layered hexagonal structure to mimic a singular liver lobule and compared against a GelMA scaffold and collagen-based dECM scaffold. An SLA technique called digital light printing (DLP) uses a digital micromirror device (DMD)-based system to rapidly polymerize each ink layer with varying mechanical properties. Ma *et al.* developed a photocrosslinkable liver-specific dECM-based hydrogel biomaterial that enhanced HepG2 cell proliferation and metabolic markers in comparison to both collagen I-based and GelMA-based scaffolds. Tuning the dECM-based scaffold stiffness to replicate a cirrhotic liver environment reduced HepG2 cell growth and viability but upregulated invasion and migration markers compared to dECM scaffolds with healthy matrix stiffness levels.<sup>55</sup> Fan *et al.* also utilized the high spatial precision of 3D bioprinting to mimic liver lobule structures using a C3A hepatocellular carcinoma cell and

HUVEC-laden GelMA bioink in DEP to pattern the hydrogel microbeads into a three-layered hexagonal structure shown in Figs. 6(a) and 6(b). This morphology, although lacking vascularization, enhanced sorafenib drug sensitivity compared to monoculture models or 3D spheroids.<sup>56</sup>

Beyond HCC recapitulation within *in vitro* models to study cancer biology, 3D bioprinting opens the door for personalized treatment plans. Xie *et al.* utilized extrusion-based bioprinting to develop a 3D-bioprinted HCC gel-SA *in vitro* model with primary tumor-derived cells. These models retained the biological and genetic profiles of the original patient tumors over the course of two to six weeks. They were used to evaluate multiple anti-cancer drug responses to tumor mutations. Although a common hydrogel, the use of gelatin and sodium alginate could not support the models for the past five months before the structures became too stiff to maintain cell viability.<sup>59</sup>

Cholangiocarcinoma (CCA) is a common intrahepatic tumor that afflicts liver bile ducts. Recent work has attempted to replicate the complexity of the CCA TME in an *in vitro* model. Mao *et al.* utilized an ALPHA-CPT1 3D bioprinter by SunP Biotech to print a  $10 \times 10 \text{ mm}^2$  six-layered CCA hydrogel model consisting of 1% sodium alginate, 30% Matrigel<sup>®</sup>, and 3.75% gelatin. The 3D scaffold demonstrated higher growth and malignancy rates, enhanced stemness, and lower drug sensitivity (sorafenib, cisplatin, and 5-fluorouracil) when compared to traditional 2D cultures.<sup>58</sup> A printed construct of CCA RBE cells surrounded by stromal cells aimed to recapitulate not only the biochemical TME cues but also the biophysical environment. Li *et al.* compared the influence of tumor-associated stromal cells on a tumor cell population. As shown in Fig. 6(c), the fabricated 3D model responded to different stromal cell roles, specifically tumor-associated fibroblasts (TAFs) and tumor-associated macrophages (TAMs) promoted malignancy and tumorigenic cell phenotypes as well as upregulation of drug-resistance

17 April 2024 13:32:23



17 April 2024 13:32:23

**FIG. 6.** Schematic to construct endothelialized liver lobule-like 3D models. (a) 3D printing process in four steps. (b) F-actin staining of cell morphology on day 1 and day 14. Scale bar = 200  $\mu\text{m}$ . (c) Schematic of 3D cholangiocarcinoma immune microenvironment. Extrusion printed RBE cell-laden hydrogel (blue) surrounded by tumor-associated stromal cell-laden hydrogel (gray). (a) and (b) are reproduced with permission from Fan *et al.*, *Micromachines* **14**(4), 878 (2023). Copyright 2023 Author(s), licensed under a Creative Commons Attribution (CC BY) license.<sup>56</sup> (c) is reproduced with permission from Li *et al.*, *Front. Immunol.* **13**, 941289 (2022). Copyright 2022 Author(s), licensed under a Creative Commons Attribution (CC BY) license.<sup>60</sup>

genes specifically through an activated Wnt/ $\beta$ -catenin pathway as a mechanism to increase tumor invasion and metastasis. The tumor-associated endothelial cells played little role in their immune tumor immune microenvironment model.<sup>60</sup>

### E. Kidney cancer model

Unlike other cancer types, few studies have recently investigated *in vitro* modeling of renal cancer utilizing 3D printing technology despite renal cell carcinoma (RCC) being within the top ten most common cancers.<sup>89</sup> One such study investigated a sub-type of RCC, papillary RCC (pRCC). Three-dimensional spheroids comprised of an inner core of patient-derived pRCC cells encased in a layer of human fibroblasts were made using magnetic bioprinting methods and maintained for 96 h. Small magnets placed beneath

each plate well-designated cell aggregation through incorporated NanoShuttle magnetic nanoparticles. In comparison to 2D monolayers, these 3D spheroids demonstrated better biological function as well as similar dose-dependent responses to capmatinib, a MET oncogene inhibitor, to published *in vivo* data.<sup>64</sup> Herrada-Manchón *et al.* developed a proof-of-concept *in vitro* model laden with RCC cells in a hydrogel disk construct to study intercellular communication and transport through tunneling nanotubes (TNTs), tiny projections that extend between neighboring cells. The 3D models were viable for at least 15 days of culture and demonstrated the ability to produce TNT-like structures, indicating the potential for cancer cell communication studies via the *in vitro* model's TNT-like projections.<sup>62</sup>

High mortality rates associated with cancer metastasis are a well-known issue. Cancer types with high migration potential are

important to study for this reason. Primary renal neuroblastomas are not common; Wu *et al.* filled the knowledge gap of tumor cells within a non-malignant renal TME. In a simplified metastasis model, an inner neuroblastoma core is surrounded by concentric layers of healthy kidney fibroblasts using a commercially available extrusion printer. Two-dimensional and three-dimensional models were compared for anti-cancer drug sensitivity and cytotoxicity using panobinostat and blastcidin, respectively. Both models displayed a clear distinction between the cancer chemotherapy drug, which mainly targeted the cancer cells, and the cytotoxic antibiotic drug, which targeted all cells present. Yet, fibroblasts within the 3D model had a lower sensitivity to the anti-cancer drug than in their respective monolayers. As previously mentioned in other studies, TME and cell type have a significant impact on drug sensitivity.<sup>63</sup> More investigations and developments of *in vitro* models are required to increase *in vitro* complexity and understanding in order to replace current animal models that, at best, produce a 3.4% successful translation from trial phase to clinical use.<sup>90</sup>

### F. Breast cancer model

The utilization of 3D printing emerged as a valuable technique in engineering breast cancer models, given its ability to exert precise spatial control over cell types, biochemical composition, and the stiffness of the printed models.<sup>2</sup> Reid *et al.* developed human mammary organoids within 3D collagen matrices through 3D bioprinting. The results showed there were superior efficiency and consistency in organoid morphology compared to manually embedded models.<sup>91</sup> Swaminathan *et al.* utilized 3D printing to create spheroids of non-tumorigenic MCF-10A and MDA-MB-231 breast cancer cells in gelatin/alginate and collagen/alginate bioinks, demonstrating enhanced resistance to paclitaxel treatment compared to 2D culture.<sup>92</sup> Wang *et al.* utilized 3D bioprinting to construct breast cancer models that closely mimic *in vivo* conditions for drug screening purposes. They printed a stromal compartment using adipose-derived mesenchymal stem cells (ADSC) and a central tumor compartment with 21PT breast cancer cells. Their findings revealed that ADSCs impeded tumor cells from undergoing apoptosis at low doxorubicin concentrations.<sup>93</sup>

With a co-extrusion-based 3D bioprinting approach as shown in Fig. 7(a), Grolman *et al.* employed human breast cancer cells (MDA-MB-231) and mouse macrophages to construct various geometries for anti-cancer drug screening.<sup>94</sup> The morphology of the 3D-printed microchannel, which accommodates macrophages at its core, was found to impact their migration behavior and interaction with breast cancer cells in the surrounding circumferential shell layer. The results showed the formation of a paracrine loop between cancer cells and macrophages, resulting in heightened motility of the macrophage cells.

### G. Breast cancer bone metastasis model

3D-printed tumor models serve as valuable tools for investigating the metastasis and invasion of breast cancer cells into bone tissue. Thibaudeau *et al.* applied melt electrospun PCL fibers seeded with primary osteoblasts to fabricate a humanized bone.<sup>95,96</sup> Subsequently, this humanized bone was implanted into mice to investigate bone metastasis. The MDA-MB-231BO cells

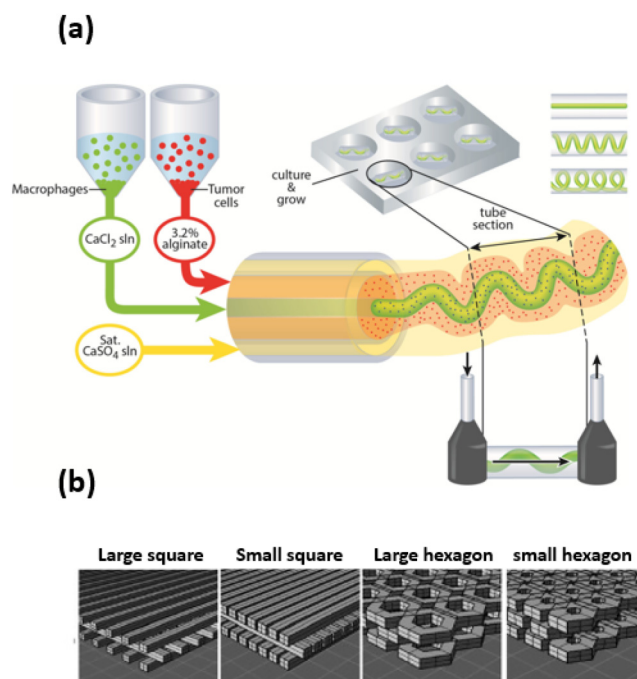


**FIG. 7.** Schematic of 3D printing techniques used for breast cancer model fabrication. (a) Involves co-bioprinting of immune cells and tumor cells, with immune cells printed as blood vessel-like channels traversing the tumor. (b) Demonstrates the capability to print scaffolds in diverse shapes using CAD. (a) is reproduced with permission from Grolman *et al.*, *Adv. Mater.* **27**(37), 5512–5517 (2015). Copyright 2015 John Wiley and Sons.<sup>94</sup> (b) is reproduced with permission from Zhu *et al.*, *Nanomed. Nanotechnol., Biol. Med.* **12**(1), 69–79 (2016). Copyright 2016 Elsevier.<sup>89</sup>

17 April 2024 13:32:23

demonstrated metastasis to the humanized bone four weeks after injection into the mice hearts. Co-culturing breast cancer cells with stromal cells from the bone microenvironment, such as MSCs and osteoblasts, is a common practice. Zhu *et al.* created PEG/hydroxyapatite (HA)-based bone mimics with a precisely controlled structure, demonstrating that cells cultured in 3D matrices exhibited increased migration compared to 2D culture. Co-culturing human fetal osteoblasts (hFOB) with breast cancer cells (MDA-MB-231) in 3D-printed matrices resulted in altered proliferation patterns, revealing increased proliferation of breast cancer cells alongside reduced proliferation of osteoblasts.<sup>97</sup> Further, the GelMA-HA system was utilized to 3D print osteoblasts and MSCs, forming the bone stromal compartment, while MDA-MB-231 cells were seeded on the matrices. This approach led to increased vascular endothelial growth factor (VEGF) expression compared to breast cells cultured in isolation.<sup>70</sup>

The majority of these investigations employed 3D printing models, where cells are not embedded in the scaffold fibers but rather seeded onto their surface. Hence, the focus is on examining the influence of scaffold geometry and composition on cancer cell proliferation, chemoresistance compared to 2D cultures, and the complex interplay between stromal and cancer cells.<sup>72,98,99</sup>

Holmes *et al.* utilized fused deposition modeling 3D printing to investigate bone colonization by breast cancer cells, using PLA-based bone scaffolds modified with carboxyl nanocrystalline HA coatings. Different scaffold patterns were explored as shown in Fig. 7(b), with small hexagonal pores proving to support the highest proliferation of breast cancer cells. This study underscored the biomimetic potential of nanosurface texturization provided by nano HA in creating a tunable bone model that mimics the complexity of native tissues.<sup>65</sup>

## H. Bone cancer model

Bone cancer, encompassing both primary and metastatic forms, is associated with high mortality and complication rates.<sup>72</sup> In pursuing more effective treatments, 3D printing and bioprinting technologies have emerged as promising avenues. These innovative approaches allow for the amalgamation of cells, biomolecules, and biomaterials, constructing intricate structures that closely emulate bone tissue's complexity. Advancements in 3D osteosarcoma models have addressed limitations inherent in traditional 2D cultures by replicating specific cues from the tumor microenvironment. Tan *et al.* used 3D printing to fabricate porous silk sponges designed for OS cell culture. This development revealed that the expression profiles of angiogenic factors more accurately mirrored those found *in vivo* tumors.<sup>100</sup> Additionally, the research led by Mano *et al.* showcased the creation of humanized 3D OS models using hydrogel, highlighting the impact of cellular arrangement and co-culture on tumor growth, invasion, and drug resistance.<sup>101</sup> In bone sarcomas, studies exploring the effects of bioceramic fillers on the proliferation and mineralization of 3D-bioprinted Saos-2 osteosarcoma cell lines have provided valuable insights into potential therapeutic interventions.<sup>71,72</sup>

## I. Lung cancer model

Biomimetic lung engineering has made some progress in recent years due to the great ability of 3D printing technology to fabricate vascularized tissues. Wang *et al.*<sup>102</sup> developed an *in vitro* lung model using 3D bioprinting for cancer research. The *in vitro* lung model with grid scaffold structures was fabricated using gelatin–sodium alginate–lung cancer cell A549/95-D suspension as the bioink. The results showed that the cells in this model are evenly viable and can be cultured for up to 28 days to maintain their structural integrity. Both A549 and 95-D cells from the 3D constructs had higher invasion and migration capability than their counterparts from the 2D culture. Thus testified, the 3D *in vitro* lung cancer model was more biomimetic and helpful for biomedical research. Ng *et al.*<sup>75</sup> applied polyvinylpyrrolidone-based bioink and a nozzle with a diameter of 300  $\mu\text{m}$  to print human three-layer alveolar lung models of various human cells. The stability and repeatability of the 3D printing process were evaluated, and the result showed that the living cells could survive and proliferate in the obtained 3D-printed models, providing a successful example for manufacturing a human alveolar lung model. Choi *et al.*<sup>17</sup> utilized a hydrogel derived from a decellularized extracellular matrix of pig lungs to create a model integrating lung cancer and idiopathic pulmonary fibrosis. In the drug-resistance assessment results, the model exhibited more significant changes in resistance

to sensitizing targeted anti-cancer drugs. This model partially reproduced the drug responsiveness of the vascularized lung cancer model with fibrosis, helping to determine appropriate treatment methods for lung cancer patients with fibrosis. The drug-resistance results showed the model partially replicated the drug sensitivity seen in the vascularized lung cancer model with fibrosis, aiding in determining suitable treatment strategies for lung cancer patients with fibrosis.

Although lung carcinoma is one of the leading causes of cancer-related death worldwide, there are still insufficient numbers of bioprinted models that have been reported to date.<sup>75</sup> Part of the reason is the lungs are a highly complex structure and it requires a further developed precision of 3D printing technology to mimic the microstructure of natural lung tissue better.<sup>103</sup> Lung tissue contains both gas exchange networks and blood supply networks. Still, the currently developed lung *in vitro* models are mainly focused on evaluating the invasion and migration ability of the cancer cells within the constructs, so more effective methods for promoting microangiogenesis should be developed.<sup>104,105</sup>

## J. Gastric cancer model

Gastric cancer was ranked the fifth most common cancer in 2020 and statistics showed that survival rate from gastric cancer remains low.<sup>106</sup> In order to biomimetic the complex digestive system of humans, Hsu *et al.* developed a gastric model which is biocompatible in terms of mechanical strength, topographical features, surface chemistry, and flow dynamics. Culture of *H. pylori* and gastric cancer MKN-45 cell line on this model showed a higher survival rate owing to the cells shielding effect of the rugae structure from fluid stress. Subsequent challenges with antibiotic and anti-cancer drugs proved that this developed 3D-printed model has the potential for high-throughput drug screening as it solves the overestimated therapeutic activity presence in the convectional 2D models.<sup>78</sup> On the other hand, Kim *et al.* constructed vascularized gastric cancer organoids for chemotherapy drug screening, particularly beneficial to those patients who show insufficient gastric cancer markers. The designed model is composed of patient-derived gastric cancer organoids (PDO), perfusable endothelium and stomach decellularized extracellular matrix. It predicts the clinical response to VEGFR2-targeted therapy in gastric cancer patients depending on the PDO molecular subtype.<sup>14</sup> Apart from the model structure design, it is also crucial to investigate fundamentally the composition of bioink which houses the cells. Similar to liver cancer model fabrication where Mao *et al.* proposed the combination of Matrigel<sup>®</sup>, sodium alginate and gelatin,<sup>58</sup> Flores-Torres *et al.* used the same material combination but at a different ratio in formulating the cell-containing bioink. It was proven that the formulated bioink allows continuous passaging where cells proliferate and reorganize into spheroids during repeating printing, harvesting, dissociation, and subsequent printing process.<sup>76</sup> Rather contrast, Kim and co-workers reported combination of cellulose nanoparticles with gastric tissue-derived decellularized extracellular matrix (g-dECM) fabricates a model with enhanced cancer-related characteristics such as cell aggregation, interaction, and drug resistance compared to conventional Matrigel<sup>®</sup> and collagen.<sup>77</sup>

17 April 2024 13:32:23



#### IV. 3D-PRINTED MICROFLUIDIC DEVICE FOR CANCER STUDY

Differing from the direct printing of cancer models as aforementioned, 3D printing techniques were also recently employed for microfluidic device printing to support cancer studies and the fabrication of tumor-on-chip devices, as summarized in Table I. In particular, the application of 3D printing in microfluidic device fabrication gained popularity as microfluidics generally benefits the research studies by reducing the amount of sample, precise handling of the sample, favorable thermodynamics, and kinetic flow, reducing the experimental duration, and mimicking *in vivo* environment.<sup>107,108</sup> 3D printing allows one-step fabrication of microfluidics and provides flexibility for feature design by simply changing the design of the CAD file.

At the early stage of cancer, detection, and quantification of circulating tumor cells were generally used for early diagnosis as they were released from the tumors. However, sensitivity and efficiency of detection often remain as challenges.<sup>109</sup> With the aid of 3D printing techniques, Chen *et al.* fabricated a microfluidic device that efficiently captures the circulating tumor cell biomarkers from peripheral blood samples. A high surface area and fluid flow design functionalized with antibodies via surface chemical modification successfully captured the circulating tumor cells at a rate of around 90%, which could be promising for clinical applications. This reveals the possibility for future complex 3D geometry structure design to improve the capture efficiencies compared to the general 2D structure.<sup>79</sup> Similar to Chen *et al.*, Park *et al.* 3D-printed a microfluidic immunomagnetic concentrator, which efficiently captured circulating tumor cells owing to the advantage of geometrical design. On top of it, this printed device further supported captured cell enrichment before feeding into the ATP luminescence assay, which improved the assay sensitivity by lowering the limit of detection. This suggests the potential of early cancer diagnosis using liquid biopsy analysis with the ATP luminescence assay.<sup>80</sup> In contrast to the two previous studies, Kadimisetty *et al.* printed an assembly of prostate cancer-targeted immunosensors.<sup>81</sup> The print was later equipped with sensor electrodes and supercapacitors to support simultaneous prostate cancer-related protein measurements. More importantly, this simple and low-cost fabricated setup reported a comparable assay result with single-protein enzyme-linked immunosorbent assays (ELISA). Such achievements foresee a promising future in adapting to other disease-related biomarkers measurement when appropriate pairs of antibodies or binding agents are identified. Similarly, Khalid *et al.* 3D-printed the microfluidic channel to support the assembly of the lung-on-chip system.<sup>82</sup> The system was then seeded with lung cancer cells and further integrated with biosensors to act as a promising tool for cytotoxicity evaluation.

On the other hand, advancements in 3D printing techniques in fabricating microstructures allow the combination of microfluidic and cell-culture technology, which leads to the idea of tumor-on-chip. For instance, Chang and co-workers highlighted the success of 3D printing techniques in heterogeneous deposition and sinusoid patterning printing to develop biomimetic liver tissue constructs within the chip system.<sup>83</sup> Following the investigation into print design, Matsusaki *et al.* proposed the layer-by-layer

alternating printing mode in constructing the 3D micro-tissue chip. It was observed that the hepatocellular function increment is dependent on the hierarchical cell-cell interaction based on the layer number and co-culture cell types.<sup>84</sup> Instead of single-cell printing, Bhise *et al.* utilized direct bioprinting of hepatocyte spheroids hydrogel construct on an easily disassembled liver-on-chip. The functionality of the bioreactor culture environment was confirmed via analysis of biomarkers [i.e., albumin, alpha-1 antitrypsin (A1AT), transferrin, and ceruloplasmin] secreted from the construct. A subsequent comparable acetaminophen treatment challenge outcome with an animal model confirmed the possibility of application for drug toxicity analysis. It showed the potential of chip systems in high-throughput drug screening.<sup>85</sup> Interestingly, Lee and Cho reported that the 3D-bioprinted liver-on-chip showed a significant enhancement in the liver function analysis (albumin and urea tests) compared to the 3D-bioprinted models using hepatocytes and hepatocytes-endothelial cells with static culture.<sup>86</sup> Apart from using the standard cells purchased from the supplier, Yi *et al.* utilized glioblastoma cells isolated from the patient for further 3D bioprinting on chip.<sup>87</sup> This approach produced a patient-specific chip system that is personalized in guiding clinical decisions. From a technical perspective, it also allows point-of-care testing in the clinical setting as production of 3D-printed glioblastoma-on-chip can be performed within a reasonable timeframe (1–2 weeks). Differing from above, where the bioprinting technique was applied to produce the 3D model/scaffold, Ji and co-workers produced a bone tumor scaffold containing lung cancer cells using stereolithography to form the dormancy niche as part of the design of pre-metastatic niche mimicking the bone-on-chip system.<sup>88</sup>

#### V. CHALLENGE AND FUTURE PERSPECTIVES

Developing an ideal *in vitro* cancer model is not straightforward. Each of the various phases of model development is a significant undertaking, and the current models still need substantial improvements to closely recapitulate the *in vivo* scenario regarding the variety of cell types involved in each cancer tumor microenvironment.<sup>110</sup> Ensuring the accurate replication of angiogenesis and the development of leaky vasculature in tumor models is crucial for maintaining sustained predictability.<sup>54</sup> Combining vasculature within 3D organotypic models alongside dynamic microfluidic platforms enriches the exploration of cancer metastasis and resistance to anti-cancer drugs. However, achieving effective integration of tumor-like vasculature mandates the utilization of high-resolution 3D printers. The meticulous selection of cell printing parameters and bioink properties is crucial to maintain the viability and phenotype of sensitive cells after the printing process.<sup>111,112</sup>

This review presents a selection of 3D-printed *in vitro* models for the most studied tumor types, illustrating the range of tissue types under investigation and techniques under development. However, there are still gaps for less well studied cancers and organ systems. Existing in *in vitro* cancer models face challenges in accurately replicating the complexities of certain types of cancers. A prominent example is the complexity of the blood-brain barrier, a unique semi-permeable membrane crucial for maintaining homeostasis within the brain. When devising *in vitro* models for brain

cancer, the incorporation of the blood-brain barrier becomes imperative for studying drug transport. Existing research on drug permeability in 3D blood-brain barrier models has been relatively limited. To bridge this gap, further investigation is required into the utilization of 3D bioprinting technology to construct platforms capable of accurately replicating the vasculature of the central nervous system, facilitating the testing and screening of drug delivery.<sup>113–115</sup>

Despite significant advancements in *in vitro* tumor model development, the current reliance on immortalized cell lines in 2D cultures may lead to responses that differ from primary cells grown in a 3D context, which better mirrors the *in vivo* scenario.<sup>116</sup> On the other side, the utilization of primary cells derived from patients presents an opportunity to distinguish unique tumor characteristics, improve the creation of personalized therapies, and refine drug evaluation. This is particularly powerful when combined with contemporary analytical tools such as next-generation sequencing or multi-omics approaches.<sup>54</sup> Additionally, primary cells can play a crucial role in conducting toxicology studies and exploring cancer initiation caused by various chemicals and lifestyle factors.<sup>117</sup>

Despite progress in 3D models for carcinogenesis, a significant number of existing models still depend on static cultures. In contrast, *in vivo* tumor cells are commonly subjected to fluid flows that substantially impact their behavior.<sup>118</sup> Therefore, upcoming models ought to integrate perfusion culture systems to closely emulate the shear forces encountered by cells *in vivo*. Furthermore, preserving a physiologic gradient of growth factors and other proteins within tissues in perfusion culture would more accurately mirror the tissue microenvironment. The incorporation of multiple cell types and the use of perfusion systems will contribute to the prolonged viability of cultures, essential for studying carcinogenic processes and developing pharmaceutical treatments.<sup>15,98,119</sup> While advancements in 3D printing have been notable in constructing *in vitro* cancer models, the predominant limitation lies in scaffold architectures, which are often confined to basic constructs such as grids. Therefore, the implementation of 3D printing methods capable of crafting more intricate architectures has the potential to augment complexity and, subsequently, more faithfully replicate the *in vivo* microenvironment.<sup>120</sup>

Although 3D printing is promising in directly printing the chip platform, particularly in forming microfluidic channels, it has still not been used to develop chips in cancer studies. In general, chip systems were mainly fabricated via poly-dimethyl siloxane (PDMS) molding using soft lithography techniques.<sup>121–123</sup> This situation could be due to the optical transparency<sup>124</sup> of PDMS, which is not achievable in 3D-printed material.<sup>79</sup> Therefore, the 3D printing technique was applied to print the mold of the PDMS cast<sup>125</sup> instead of printing the chip device directly.

Despite the challenges outlined earlier, the 3D printing of human-relevant *in vitro* cancer models has the potential to overcome the limitations associated with 2D culture and animal *in vivo* models. The opportunity to surmount current obstacles rests in an interdisciplinary collaboration that converges disciplines like biological, mechanical, chemical, and electrical science. This collective effort, combined with advancements in 3D printing technology, holds the potential to establish 3D-printed *in vitro* models as dependable tools for drug screening and to deepen our comprehension of the fundamental mechanisms contributing to carcinogenesis.

## ACKNOWLEDGMENTS

B.Z. and S.E. would like to thank Brunel Research Interdisciplinary Labs (BRIL) and Brief Award (BRIEF) for supporting the research work and collaborations.

## AUTHOR DECLARATIONS

### Conflict of Interest

The authors have no conflicts to disclose.

## Author Contributions

B. Z., M. M., and X.Y.T. contributed equally to this work.

**Bin Zhang:** Conceptualization (equal); Writing – original draft (equal); Writing – review & editing (equal). **Meagan Morgan:** Writing – original draft (equal); Writing – review & editing (equal). **Xin Yi Teoh:** Writing – original draft (equal); Writing – review & editing (equal). **Ruth Mackay:** Writing – review & editing (equal). **Sibylle Ermler:** Writing – review & editing (equal). **Roger Narayan:** Conceptualization (equal); Writing – review & editing (equal).

## DATA AVAILABILITY

The data that support the findings of this study are available within the article.

## REFERENCES

- 1 D. Sia, A. Moeini, I. Labгаа, and A. Villanueva, *Pharmacogenomics* **16**(14), 1671–1683 (2015).
- 2 G. Bahcecioglu, G. Basara, B. W. Ellis, X. Ren, and P. Zorlutuna, *Acta Biomater.* **106**, 1–21 (2020).
- 3 T. Denayer, T. Stöhr, and M. Van Roy, *New Horiz. Transl. Med.* **2**(1), 5–11 (2014).
- 4 I. W. Mak, N. Evaniew, and M. Ghert, *Am. J. Transl. Res.* **6**(2), 114 (2014); available at <https://www.ncbi.nlm.nih.gov/pmc/articles/PMC3902221/>
- 5 H. Samadian, S. Jafari, M. Sepand, L. Alaei, S. S. Malvajerd, M. Jaymand, F. Ghobadinezhad, F. Jahanshahi, M. Hamblin, and H. Derakhshankhah, *Mater. Today Adv.* **12**, 100160 (2021).
- 6 R. Augustine, S. N. Kalva, R. Ahmad, A. A. Zahid, S. Hasan, A. Nayeem, L. McClements, and A. Hasan, *Transl. Oncol.* **14**(4), 101015 (2021).
- 7 S. Samavedi and N. Joy, *Curr. Opin. Biomed. Eng.* **2**, 35–42 (2017).
- 8 M. Cavo, F. Serio, N. R. Kale, E. D'Amone, G. Gigli, and L. L. Del Mercato, *Biomater. Sci.* **8**(18), 4887–4905 (2020).
- 9 S. Chen, S. K. Boda, S. K. Batra, X. Li, and J. Xie, *Adv. Healthcare Mater.* **7**(6), 1701024 (2018).
- 10 X. Xu, M. C. Farach-Carson, and X. Jia, *Biotechnol. Adv.* **32**(7), 1256–1268 (2014).
- 11 A. Sola, J. Bertacchini, D. D'Avella, L. Anselmi, T. Maraldi, S. Marmiroli, and M. Messori, *Mater. Sci. Eng. C* **96**, 153–165 (2019).
- 12 B. Zhang, P. Belton, X. Y. Teoh, A. Gleadall, R. Bibb, and S. Qi, *J. Mater. Chem. B* **12**(1), 131–144 (2024).
- 13 B. Zhang, J. Huang, and R. J. Narayan, *J. Mater. Chem. B* **8**(36), 8149–8170 (2020).
- 14 J. Kim, J. Kim, G. Gao, Y. M. Choi, J. Kim, D. W. Cho, J. H. Cheong, and J. Jang, *Adv. Funct. Mater.* **56**(12), 4431–4446 (2023).
- 15 B. Zhang, *Proc. Struct. Integr.* **49**, 3–9 (2023).
- 16 S. Qi, B. Zhang, and T. McDonagh, in *Implantable technologies* (Royal Society of Chemistry, 2021), pp. 252–295.

- <sup>17</sup>Y.-M. Choi, H. Lee, M. Ann, M. Song, J. Rheey, and J. Jang, *Biofabrication* **15**(3), 034104 (2023).
- <sup>18</sup>H. Sun, L. Sun, X. Ke, L. Liu, C. Li, B. Jin, P. Wang, Z. Jiang, H. Zhao, and Z. Yang, *Adv. Sci.* **11**(2), 2304460 (2023).
- <sup>19</sup>A. Cano-Vicent, M. M. Tambuwala, S. S. Hassan, D. Barh, A. A. Aljabali, M. Birkett, A. Arjunan, and Á Serrano-Aroca, *Addit. Manuf.* **47**, 102378 (2021).
- <sup>20</sup>S. Singh, G. Singh, C. Prakash, and S. Ramakrishna, *J. Manuf. Processes* **55**, 288–306 (2020).
- <sup>21</sup>B. Zhang, A. Gleadall, P. Belton, T. McDonagh, R. Bibb, and S. Qi, *Addit. Manuf.* **46**, 102196 (2021).
- <sup>22</sup>S. V. Murphy and A. Atala, *Nat. Biotechnol.* **32**(8), 773–785 (2014).
- <sup>23</sup>B. Zhang, R. Cristescu, D. B. Chrisey, and R. J. Narayan, *Int. J. Bioprinting* **6**(1), 211 (2020).
- <sup>24</sup>R. F. Pereira and P. J. Bártolo, *J. Appl. Polym. Sci.* **132**(48), 1–15 (2015).
- <sup>25</sup>S. Azizi Macheqposhti, B. Zhang, R. Sachan, L. Vanderwal, S. J. Stafslien, and R. J. Narayan, *J. Mater. Res.* **36**, 3865–3876 (2021).
- <sup>26</sup>Q. Ge, Z. Li, Z. Wang, K. Kowsari, W. Zhang, X. He, J. Zhou, and N. X. Fang, *Int. J. Extreme Manuf.* **2**(2), 022004 (2020).
- <sup>27</sup>F. P. Melchels, J. Feijen, and D. W. Grijpma, *Biomaterials* **31**(24), 6121–6130 (2010).
- <sup>28</sup>R. Kostecki, A. Arman, B. Zhang, K. H. Yang, R. J. Narayan, M. R. Hutchinson, and H. Eberdorff-Heidepriem, *Med. Devices Sens.* **3**(6), e10135 (2020).
- <sup>29</sup>D. A. Foyt, M. D. Norman, T. T. Yu, and E. Gentleman, *Adv. Healthcare Mater.* **7**(8), 1700939 (2018).
- <sup>30</sup>B. Zhang, X. Y. Teoh, J. Yan, A. Gleadall, P. Belton, R. Bibb, and S. Qi, *Int. J. Pharm.* **625**, 122140 (2022).
- <sup>31</sup>R. Winarso, P. Anggoro, R. Ismail, J. Jamari, and A. Bayuseno, *Heliyon* **8**, 1–14 (2022).
- <sup>32</sup>T. D. Ngo, A. Kashani, G. Imbalzano, K. T. Nguyen, and D. Hui, *Compos. Part B Eng.* **143**, 172–196 (2018).
- <sup>33</sup>F. M. Mwema, E. T. Akinlabi, F. M. Mwema, and E. T. Akinlabi, in *Fused deposition modeling: Strategies for quality enhancement* (Springer, 2020), pp. 1–15; available at <https://link.springer.com/book/10.1007/978-3-030-48259-6>
- <sup>34</sup>K. Hölzl, S. Lin, L. Tytgat, S. Van Vlierberghe, L. Gu, and A. Ovsianikov, *Biofabrication* **8**(3), 032002 (2016).
- <sup>35</sup>B. Guillotin, A. Souquet, S. Catros, M. Duocastella, B. Pippenger, S. Bellance, R. Bareille, M. Rémy, L. Bordenave, and J. Amédée, *Biomaterials* **31**(28), 7250–7256 (2010).
- <sup>36</sup>V. Keriquel, H. Oliveira, M. Rémy, S. Ziane, S. Delmond, B. Rousseau, S. Rey, S. Catros, J. Amédée, and F. Guillemot, *Sci. Rep.* **7**(1), 1778 (2017).
- <sup>37</sup>A. Al Rashid, W. Ahmed, M. Y. Khalid, and M. Koc, *Addit. Manuf.* **47**, 102279 (2021).
- <sup>38</sup>D. Hakobyan, C. Medina, N. Dusserre, M.-L. Stachowicz, C. Handschin, J.-C. Fricain, J. Guillermet-Guibert, and H. Oliveira, *Biofabrication* **12**(3), 035001 (2020).
- <sup>39</sup>B. Huang, X. Wei, K. Chen, L. Wang, and M. Xu, *Int. J. Bioprinting* **9**(3), 1–13 (2023); available at <https://www.ncbi.nlm.nih.gov/pmc/articles/PMC10236328/>
- <sup>40</sup>R. H. Utama, V. T. Tan, K. C. Tjandra, A. Sexton, D. H. Nguyen, A. P. O'Mahony, E. Y. Du, P. Tian, J. C. Ribeiro, and M. Kavallaris, *Macromol. Biosci.* **21**(9), 2100125 (2021).
- <sup>41</sup>A. Habib, V. Sathish, S. Mallik, and B. Khoda, *Materials* **11**(3), 454 (2018).
- <sup>42</sup>N. R. de Barros, A. Gomez, M. Ermis, N. Falcone, R. Haghniaz, P. Young, Y. Gao, A.-F. Aquino, S. Li, and S. Niu, *Biofabrication* **15**(4), 045005 (2023).
- <sup>43</sup>W. Xu, X. Zhang, P. Yang, O. Långvik, X. Wang, Y. Zhang, F. Cheng, M. Österberg, S. Willför, and C. Xu, *ACS Appl. Mater. Interfaces* **11**(13), 12389–12400 (2019).
- <sup>44</sup>E. M. Langer, B. L. Allen-Petersen, S. M. King, N. D. Kendsersky, M. A. Turnidge, G. M. Kuziel, R. Riggers, R. Samatham, T. S. Amery, and S. L. Jacques, *Cell Rep.* **26**(3), 608–623.e6 (2019).
- <sup>45</sup>H. Chen, Y. Cheng, X. Wang, J. Wang, X. Shi, X. Li, W. Tan, and Z. Tan, *Theranostics* **10**(26), 12127 (2020).
- <sup>46</sup>J. Rios De La Rosa, J. Wubetu, N. Tirelli, and A. Tirella, *Biomed. Phys. Eng. Express* **4**(4), 045010 (2018).
- <sup>47</sup>C. McGuckin, N. Forraz, C. Milet, M. Lacroix, Y. Sbirkov, V. Sarafian, C. Ebel, A. Spindler, V. Koerper, and J.-M. Balloul, *Cancers* **15**(19), 4724 (2023).
- <sup>48</sup>Y. Zhang, Z. Wang, Q. Hu, H. Luo, B. Lu, Y. Gao, Z. Qiao, Y. Zhou, Y. Fang, and J. Gu, *Small* **18**(18), 2200364 (2022).
- <sup>49</sup>Y. Sbirkov, D. Molander, C. Milet, I. Bodurov, B. Atanasov, R. Penkov, N. Belev, N. Forraz, C. McGuckin, and V. Sarafian, *Front. Bioeng. Biotechnol.* **9**, 910 (2021).
- <sup>50</sup>F. Meng, C. M. Meyer, D. Joung, D. A. Vallera, M. C. McAlpine, and A. Panoskaltis-Mortari, *Adv. Mater.* **31**(10), 1806899 (2019).
- <sup>51</sup>S. K. Schmidt, R. Schmid, A. Arkudas, A. Kengelbach-Weigand, and A. K. Bosserhoff, *Cells* **8**(10), 1295 (2019).
- <sup>52</sup>S. Sang, X. Wang, J. Duan, Y. Cao, Z. Shen, L. Sun, Q. Duan, and Z. Liu, *Biotechnol. Bioeng.* **120**(10), 2853–2864 (2023).
- <sup>53</sup>D. S. Reynolds, I. de Lázaro, M. L. Blache, Y. Liu, N. C. Jeffreys, R. M. Doolittle, E. Grandidier, J. Olszewski, M. T. Dacus, and D. J. Mooney, *Adv. Mater.* **35**(33), 2210748 (2023).
- <sup>54</sup>J. R. Browning, P. Derr, K. Derr, N. Doudican, S. Michael, S. R. Lish, N. A. Taylor, J. G. Krueger, M. Ferrer, and J. A. Carucci, *Oncotarget* **11**(27), 2587 (2020).
- <sup>55</sup>X. Ma, C. Yu, P. Wang, W. Xu, X. Wan, C. S. E. Lai, J. Liu, A. Koroleva-Maharajh, and S. Chen, *Biomaterials* **185**, 310–321 (2018).
- <sup>56</sup>Z. Fan, X. Wei, K. Chen, L. Wang, and M. Xu, *Micromachines* **14**(4), 878 (2023).
- <sup>57</sup>L. Sun, H. Yang, Y. Wang, X. Zhang, B. Jin, F. Xie, Y. Jin, Y. Pang, H. Zhao, and X. Lu, *Front. Oncol.* **10**, 878 (2020).
- <sup>58</sup>S. Mao, J. He, Y. Zhao, T. Liu, F. Xie, H. Yang, Y. Mao, Y. Pang, and W. Sun, *Biofabrication* **12**(4), 045014 (2020).
- <sup>59</sup>F. Xie, L. Sun, Y. Pang, G. Xu, B. Jin, H. Xu, X. Lu, Y. Xu, S. Du, and Y. Wang, *Biomaterials* **265**, 120416 (2021).
- <sup>60</sup>C. Li, B. Jin, H. Sun, Y. Wang, H. Zhao, X. Sang, H. Yang, and Y. Mao, *Front. Immunol.* **13**, 941289 (2022).
- <sup>61</sup>Y. Li, T. Zhang, Y. Pang, L. Li, Z.-N. Chen, and W. Sun, *Biofabrication* **11**(3), 034102 (2019).
- <sup>62</sup>H. Herrada-Manchón, L. Celada, D. Rodríguez-González, M. A. Fernandez, E. Aguilar, and M.-D. Chiara, *Mater. Sci. Eng. C* **128**, 112357 (2021).
- <sup>63</sup>D. Wu, J. Berg, B. Arlt, V. Röhrs, M. A. Al-Zeer, H. E. Deubzer, and J. Kurreck, *Int. J. Mol. Sci.* **23**(1), 122 (2021).
- <sup>64</sup>K. A. Rosette, S. M. Lander, C. VanOpstall, and B. D. Looyenga, *Am. J. Physiol. Renal Physiol.* **321**(1), F33–F46 (2021).
- <sup>65</sup>B. Holmes, W. Zhu, and L. G. Zhang, *MRS Online Proc. Library* **1724**, mrsf14-1724-h1709-1703 (2014).
- <sup>66</sup>K. Lv, J. Zhu, S. Zheng, Z. Jiao, Y. Nie, F. Song, T. Liu, and K. Song, *Mater. Sci. Eng. C* **119**, 111509 (2021).
- <sup>67</sup>J. Han, S. Jeon, M. K. Kim, W. Jeong, J. J. Yoo, and H.-W. Kang, *Biofabrication* **14**(3), 034102 (2022).
- <sup>68</sup>P. Barros da Silva, M. Coelho, S. J. Bidarra, S. C. Neves, and C. C. Barrias, *Front. Bioeng. Biotechnol.* **8**, 494 (2020).
- <sup>69</sup>W. Zhu, B. Holmes, R. I. Glazer, and L. G. Zhang, *Nanomed. Nanotechnol. Biol. Med.* **12**(1), 69–79 (2016).
- <sup>70</sup>X. Zhou, W. Zhu, M. Nowicki, S. Miao, H. Cui, B. Holmes, R. I. Glazer, and L. G. Zhang, *ACS Appl. Mater. Interfaces* **8**(44), 30017–30026 (2016).
- <sup>71</sup>X. Wang, E. Tolba, H. C. Schröder, M. Neufurth, Q. Feng, B. Diehl-Seifert, and W. E. Müller, *PLoS One* **9**(11), e112497 (2014).
- <sup>72</sup>T. Fischetti, G. Di Pompo, N. Baldini, S. Avnet, and G. Graziani, *Cancers* **13**(16), 4065 (2021).
- <sup>73</sup>M.-L. Wang, N.-Y. Xu, R.-Z. Tang, and X.-Q. Liu, *Mater. Today Bio* **15**, 10222 (2022).
- <sup>74</sup>X. Wang, X. Zhang and X. Dai, (2018).
- <sup>75</sup>W. L. Ng, T. C. Ayi, Y.-C. Liu, S. L. Sing, W. Y. Yeong, and B.-H. Tan, *Int. J. Bioprinting* **7**(2), 53–67 (2021).

- <sup>76</sup>S. Flores-Torres, O. Peza-Chavez, H. Kuasne, J. G. Munguia-Lopez, J. Kort-Mascort, L. Ferri, T. Jiang, C. V. Rajadurai, M. Park, V. Sangwan, and J. M. Kinsella, *Biofabrication* **13**(2), 1–12 (2021).
- <sup>77</sup>J. Kim, J. Jang, and D. W. Cho, *Front. Bioeng. Biotechnol.* **9**, 1 (2021).
- <sup>78</sup>Y. T. Hsu, S. P. Lee, C. H. Li, M. H. Ho, and C. Y. Kao, "Preparation of 3D-printed gastric models with biomimetic mechanical, topographical and fluid dynamic properties," *J. Taiwan Inst. Chem. Eng.* (published online, 2024).
- <sup>79</sup>J. Chen, C. Y. Liu, X. Wang, E. Sweet, N. Liu, X. Gong, and L. Lin, *Biosens. Bioelectron.* **150**, 111900 (2020).
- <sup>80</sup>C. Park, A. T. Abafogi, D. V. Ponnuruvelu, I. Song, K. Ko, and S. Park, *Biosensors* **11**(8), 278 (2021).
- <sup>81</sup>K. Kadimisetty, I. M. Mosa, S. Malla, J. E. Satterwhite-Warden, T. M. Kuhns, R. C. Faria, N. H. Lee, and J. F. Rusling, *Biosens. Bioelectron.* **77**, 188–193 (2016).
- <sup>82</sup>M. A. U. Khalid, Y. S. Kim, M. Ali, B. G. Lee, Y. J. Cho, and K. H. Choi, *Biochem. Eng. J.* **155**, 15 (2020).
- <sup>83</sup>R. Chang, K. Emami, H. Wu, and W. Sun, *Biofabrication* **2**(4), 045004 (2010).
- <sup>84</sup>M. Matsusaki, K. Sakaue, K. Kadowaki, and M. Akashi, *Adv. Healthcare Mater.* **2**(4), 534–539 (2013).
- <sup>85</sup>N. S. Bhise, V. Manoharan, S. Massa, A. Tamayol, M. Ghaderi, M. Miscuglio, Q. Lang, Y. Shrike Zhang, S. R. Shin, G. Calzone, N. Annabi, T. D. Shupe, C. E. Bishop, A. Atala, M. R. Dokmeci, and A. Khademhosseini, *Biofabrication* **8**(1), 014101 (2016).
- <sup>86</sup>H. Lee and D. W. Cho, *Lab Chip* **16**(14), 2618–2625 (2016).
- <sup>87</sup>H. G. Yi, Y. H. Jeong, Y. Kim, Y. J. Choi, H. E. Moon, S. H. Park, K. S. Kang, M. Bae, J. Jang, H. Youn, S. H. Paek, and D. W. Cho, *Nat. Biomed. Eng.* **3**(7), 509–519 (2019).
- <sup>88</sup>X. Ji, H. P. Bei, G. Zhong, H. Shao, X. He, X. Qian, Y. Zhang, and X. Zhao, *Small* **19**(49), 2207606 (2023).
- <sup>89</sup>K. A. Rosette, S. M. Lander, C. VanOpstall, and B. D. Looyenga, *Am. J. Physiology-Renal Physiology* **321**(1), F33–F46 (2021).
- <sup>90</sup>C. H. Wong, K. W. Siah, and A. W. Lo, *Biostatistics* **20**(2), 273–286 (2019).
- <sup>91</sup>J. A. Reid, P. A. Mollica, R. D. Bruno, and P. C. Sachs, *Breast Cancer Res.* **20**(1), 1–13 (2018).
- <sup>92</sup>S. Swaminathan, Q. Hamid, W. Sun, and A. M. Clyne, *Biofabrication* **11**(2), 025003 (2019).
- <sup>93</sup>Y. Wang, W. Shi, M. Kuss, S. Mirza, D. Qi, A. Krasnoslobodtsev, J. Zeng, H. Band, V. Band, and B. Duan, *ACS Biomater. Sci. Eng.* **4**(12), 4401–4411 (2018).
- <sup>94</sup>J. M. Grolman, D. Zhang, A. M. Smith, J. S. Moore, and K. A. Kilian, *Adv. Mater.* **27**(37), 5512–5517 (2015).
- <sup>95</sup>L. Thibaudeau, A. V. Taubenberger, B. M. Holzapfel, V. M. Quent, T. Fuehrmann, P. Hesami, T. D. Brown, P. D. Dalton, C. A. Power, and B. G. Hollier, *Dis. Mod. Mech.* **7**(2), 299–309 (2014).
- <sup>96</sup>V. Quent, A. Taubenberger, J. Reichert, L. Martine, J. Clements, D. Huttmacher, and D. Loessner, *J. Tissue Eng. Regen. Med.* **12**(2), 494–504 (2018).
- <sup>97</sup>W. Zhu, N. J. Castro, H. Cui, X. Zhou, B. Boualam, R. McGrane, R. I. Glazer, and L. G. Zhang, *Nanotechnology* **27**(31), 315103 (2016).
- <sup>98</sup>W. H. Abuwafa, W. G. Pitt, and G. A. Hussein, *J. Biomed. Sci.* **31**(1), 7 (2024).
- <sup>99</sup>Y. Li, J. Liu, S. Xu, and J. Wang, *Int. J. Nanomed.* **18**, 8039–8057 (2023).
- <sup>100</sup>P. H. Tan, K. Aung, S. Toh, J. C. Goh, and S. Nathan, *Biomaterials* **32**(26), 6131–6137 (2011).
- <sup>101</sup>C. F. Monteiro, C. A. Custódio, and J. F. Mano, *Acta Biomater.* **134**, 204–214 (2021).
- <sup>102</sup>X. Wang, X. Zhang, X. Dai, X. Wang, X. Li, J. Diao, and T. Xu, *3 Biotech.* **8**, 1–9 (2018).
- <sup>103</sup>M. G. Sánchez-Salazar, M. M. Álvarez, and G. Trujillo-de Santiago, *Bioprinting* **21**, e00120 (2021).
- <sup>104</sup>K. Zheng, M. Chai, B. Luo, K. Cheng, Z. Wang, N. Li, and X. Shi, *Smart Mater. Med.* **5**, 183–195 (2024).
- <sup>105</sup>M. Barreiro Carpio, M. Dabaghi, J. Ungureanu, M. R. Kolb, J. A. Hirota, and J. M. Moran-Mirabal, *Front. Bioeng. Biotechnol.* **9**, 773511 (2021).
- <sup>106</sup>E. Morgan, M. Arnold, M. C. Camargo, A. Gini, A. T. Kunzmann, T. Matsuda, F. Meheus, R. H. A. Verhoeven, J. Vignat, M. Laversanne, J. Ferlay, and I. Soerjomataram, *eClinicalMedicine* **47**, 1 (2022).
- <sup>107</sup>C. Chen, B. T. Mehl, A. S. Munshi, A. D. Townsend, D. M. Spence, and R. S. Martin, *Anal. Methods* **8**(31), 6005–6012 (2016).
- <sup>108</sup>M. M. Prabhakar, A. Saravanan, A. H. Lenin, K. Mayandi, and P. S. Ramalingam, *Mater. Today Proc.* **45**, 6108–6114 (2021).
- <sup>109</sup>V. Akpe, T. H. Kim, C. L. Brown, and I. E. Cock, *J. R. Soc. Interface* **17**(168), 20200065 (2020).
- <sup>110</sup>M. E. Katt, A. L. Placone, A. D. Wong, Z. S. Xu, and P. C. Searson, *Front. Bioeng. Biotechnol.* **4**, 12 (2016).
- <sup>111</sup>F. Salamanna, D. Contartese, M. Maglio, and M. Fini, *Oncotarget* **7**(28), 44803 (2016).
- <sup>112</sup>C. R. Ireson, M. S. Alavijeh, A. M. Palmer, E. R. Fowler, and H. J. Jones, *Br. J. Cancer* **121**(2), 101–108 (2019).
- <sup>113</sup>D. H. Upton, C. Ung, S. M. George, M. Tsoli, M. Kavallaris, and D. S. Ziegler, *Theranostics* **12**(10), 4734 (2022).
- <sup>114</sup>R. Baghban, L. Roshangar, R. Jahanban-Esfahlan, K. Seidi, A. Ebrahimi-Kalan, M. Jaymand, S. Kolahian, T. Javaheri, and P. Zare, *Cell Commun. Signaling* **18**, 1–19 (2020).
- <sup>115</sup>L. Yan, R. A. Moriarty, and K. M. Stroka, *Theranostics* **11**(20), 10148 (2021).
- <sup>116</sup>M. Kapalczyńska, T. Kolenda, W. Przybyła, M. Zajączkowska, A. Teresiak, V. Filas, M. Ibs, R. Bliźniak, Ł. Łuczewski, and K. Lamperska, *Arch. Med. Sci.* **14**(4), 910–919 (2018).
- <sup>117</sup>E. M. Tosca, D. Ronchi, D. Facciolo, and P. Magni, *Biomedicines* **11**(4), 1058 (2023).
- <sup>118</sup>M. E. Bregenzler, E. N. Horst, P. Mehta, C. M. Novak, S. Raghavan, C. S. Snyder, and G. Mehta, *PLoS One* **14**(5), e0216564 (2019).
- <sup>119</sup>K. Poornima, A. P. Francis, M. Hoda, M. A. Eladl, S. Subramanian, V. P. Veeraghavan, M. El-Sherbiny, S. M. Asseri, A. B. A. Hussamuldin, and K. M. Surapaneni, *Front. Oncol.* **12**, 891673 (2022).
- <sup>120</sup>E. Cauli, M. A. Polidoro, S. Marzorati, C. Bernardi, M. Rasponi, and A. Lleo, *J. Biol. Eng.* **17**(1), 53 (2023).
- <sup>121</sup>Y. Chen, D. Gao, Y. Wang, S. Lin, and Y. Jiang, *Anal. Chim. Acta* **1036**, 97–106 (2018).
- <sup>122</sup>N. V. Menon, Y. J. Chuah, B. Cao, M. Lim, and Y. Kang, *Biomicrofluidics* **8**(6), 064118 (2014).
- <sup>123</sup>J. Aleman and A. Skardal, *Biotechnol. Bioeng.* **116**(4), 936–944 (2019).
- <sup>124</sup>V. Faustino, S. O. Catarino, R. Lima, and G. Minas, *J. Biomech.* **49**(11), 2280–2292 (2016).
- <sup>125</sup>J. Shrestha, M. Ghadiri, M. Shanmugavel, S. Razavi Bazaz, S. Vasilescu, L. Ding, and M. Ebrahimi Warkiani, *Organs Chip* **1**, 100001 (2019).